The Journal of Organic Chemistry

UCSF Library

Subscriber access provided by - Access paid by the | UCSF Library

Article

Development of a Class of Easily Scalable, Electron-Deficient, Core-Extended Benzo-Fused Azadipyrromethene Derivatives

Yuriy V. Zatsikha, Liliya I. Shamova, Tanner S. Blesener, Ilya A. Kuzmin,
Yaroslaw V. Germanov, David E. Herbert, and Victor N. Nemykin

J. Org. Chem., **Just Accepted Manuscript** • DOI: 10.1021/acs.joc.9b02074 • Publication Date (Web): 02 Oct 2019

Downloaded from pubs.acs.org on October 7, 2019

Just Accepted

"Just Accepted" manuscripts have been peer-reviewed and accepted for publication. They are posted online prior to technical editing, formatting for publication and author proofing. The American Chemical Society provides "Just Accepted" as a service to the research community to expedite the dissemination of scientific material as soon as possible after acceptance. "Just Accepted" manuscripts appear in full in PDF format accompanied by an HTML abstract. "Just Accepted" manuscripts have been fully peer reviewed, but should not be considered the official version of record. They are citable by the Digital Object Identifier (DOI®). "Just Accepted" is an optional service offered to authors. Therefore, the "Just Accepted" Web site may not include all articles that will be published in the journal. After a manuscript is technically edited and formatted, it will be removed from the "Just Accepted" Web site and published as an ASAP article. Note that technical editing may introduce minor changes to the manuscript text and/or graphics which could affect content, and all legal disclaimers and ethical guidelines that apply to the journal pertain. ACS cannot be held responsible for errors or consequences arising from the use of information contained in these "Just Accepted" manuscripts.

is published by the American Chemical Society. 1155 Sixteenth Street N.W.,
Washington, DC 20036

Published by American Chemical Society. Copyright © American Chemical Society.
However, no copyright claim is made to original U.S. Government works, or works
produced by employees of any Commonwealth realm Crown government in the course
of their duties.

Development of a Class of Easily Scalable, Electron-Deficient, Core-Extended *Benzo*-Fused Azadipyrromethene Derivatives (“MB-DIPY”)

Yuriy V. Zatsikha,*,† Liliya I. Shamova,† Tanner S. Blesener,† Ilya A. Kuzmin,† Yaroslaw V. Germanov,† David E. Herbert,† Victor N. Nemykin,*,†

†Department of Chemistry, University of Manitoba, Winnipeg, MB, R3T 2N2, Canada

KEYWORDS. aza-BODIPY, BODIPY, azadipyrromethene, phthalonitrile, electron-deficient chromophore, isoindolin-1-imines

ABSTRACT: We have developed a new synthetic strategy for the preparation of a series of isoindolin-1-imines and isoindolin-1-ones from aromatic ketones and phthalonitrile. Self-condensation reactions of these isoindolin-1-imines led to the formation of a novel class of *benzo*-fused, highly electron-deficient core-extended azadipyrromethene chromophores (“MB-DIPY”). The influence of temperature, catalyst, and the template ions, on the self-condensation reaction rate, yield, and stereoselectivity, was examined in detail. New chromophores (sodium, zinc, and metal-free compounds) were characterized by NMR, UV-Vis, fluorescence, high-resolution mass spectroscopies, and in many cases, X-ray crystallography. Their redox properties were probed by electrochemical and spectroelectrochemical approaches that revealed the remarkable electron-accepting nature of the new systems. Stepwise one- and two-electron reduction of the new MB-DIPYs and their zinc complexes was investigated by spectroscopic and spectroelectrochemical methods. Both one- and two-electron reduced forms of all zinc complexes studied have strong absorption in the NIR region up to ~1200 nm. An unusual spectroscopic and electrochemical properties of these dyes were correlated with their electronic structures and excited state natures predicted by Density Functional Theory (DFT) and Time-Dependent DFT calculations. Despite some structural similarities with well-known aza-BODIPYs, the new MB-DIPYs differ remarkably from them in spectroscopic and redox properties.

INTRODUCTION

Besides traditional use as pigments and colorants, functional dyes have proven to be useful systems in catalysis, photodynamic cancer and antibacterial therapies, sensing, imaging, and molecular electronics. In particular, phthalocyanines (Pcs) and their analogs[1-7] as well as more recent BODIPYs,[8-12] aza-BODIPYs,[13-18] and BOPHYs[19-23] have been intensively studied as easily tunable universal platforms for a variety of applications. Phthalonitrile (**1**) is one of the most popular precursors for making organic dyes, such as Pcs,[24] aza-BODIPYs,[25] subphthalocyanines,[26] and “half”-Pcs[27] (Chart 1). It is well known, that upon the treatment with ammonia, phthalonitrile can also be converted into its more reactive form – a 1,3-diiminoisoindoline (DII) heterocycle, often a more desirable precursor for preparation of organic dyes.[28-30] Thus, a variety of substituted 1,3-diiminoisoindoline derivatives can be found in the literature.[24,31] In comparison, the number of 3-alkylidene-1-iminoisoindolines(ones) derivatives is limited, and their syntheses tend to be more complicated compared to with DII.[32] Since the isoindolinone fragment is an integral part of many naturally occurring products,[33,34] its derivatives attract significant synthetic interest as a pharmacological scaffolds in medicinal chemistry.[35-38] An improvement in the synthesis of 3-alkylidene-isoindol-1-ones has been made in recent years, and a few alternative methods developed as well. For instance, some 3-alkylidene-isoindolin-1-ones were prepared starting from the thionation of phthalimide followed by alkylation with α-bromoketones,[39] by the palladium-catalyzed condensation of *o*-iodobenzamides with terminal alkynes,[40] through the aromatic heteroannulation *via* ortho lithiation-cyclization of *N*-acyl-2-bromobenzamides,[41] by the reaction of electron-deficient alkynes with *N*-hydroxyphthalimides.[42]

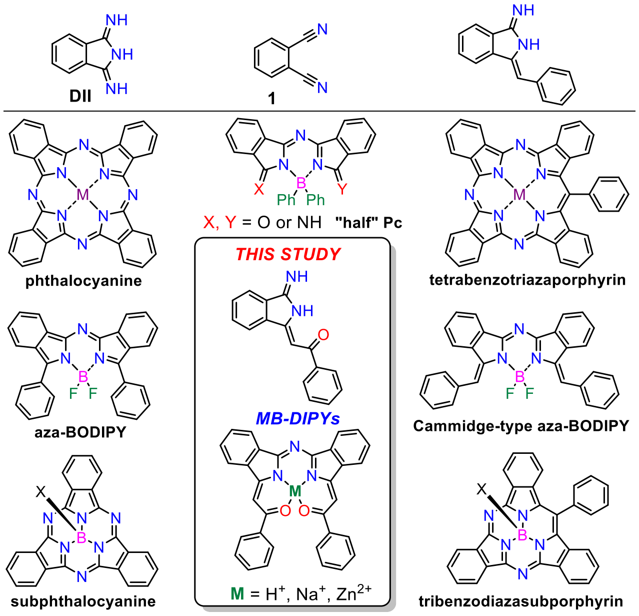

Chart 1. Selected examples of traditional aromatic macrocycles, hybrid structures, and new compounds from this study.[24-27,43-48]

At the same time, a very limited number of synthetic strategies have been proposed for the synthesis of isoindol-1-imine derivatives,[43,44] with, to the best of our knowledge, only one method reported for the preparation of 3-alkylidene-isoindol-1-imine:[45] the microwave assisted, palladium-catalyzed reaction of 2-bromobenzamide with phenylacetylene. Cammidge and coworkers recently described the synthesis of new hybrid *meso*-substituted tetrabenzotriazaporphyrins,[46] new hybrid boron subphthalocyanine–subporphyrin systems[47] as well as aza-BODIPY type compounds[48] starting from such isoindol-1-imines (Chart 1).

The development of new synthetic methodologies for preparation of a large variety of the 3-alkylidene-isoindol-1-imines is therefore both a promising and challenging task that could lead to the discovery of new hybrid chromophoric systems. It is known that under strongly basic conditions, phthalonitrile undergoes an *ortho*-hydrogen deprotonation reaction, which leads to the formation of asymmetric *benzo*-fused azadipyrromethene-type compounds.[49] This unusual side reaction is very likely the main reason a limited number of 3-alkylidene-isoindol-1-imines have been reported in the literature so far. The only known exception is the reaction of Grignard reagents with the phthalonitrile, which can be used for the synthesis of *benzo*-fused azadipyrromethenes.[50,51] However, this route is limited to aromatic magnesium halides.[52,53] Herein, we report a new synthetic strategy for the preparation of 3-alkylidene-isoindol-1-imines(ones). These precursors were found to undergo a self-condensation reaction that leads to the formation of an unprecedented class of a highly electron-deficient *benzo*-fused core-extended azadipyrromethene systems ("MB-DIPYs", Chart 1). These new chromophores can be reversibly reduced into traditional aza-DIPY type chromophores that have intense and rich NIR absorption and fluorescence properties.

RESULTS AND DISCUSSION

Synthesis

Following our recent findings on the condensation of DII with organic CH-acids that resulted in the formation of 1,3-bis-alkylidene-isoindole-based chromophores,[54,55] we decided to explore the reactivity of the phthalonitrile **1** towards other carbon-centered nucleophiles. As the CH-acid precursors, we chose a series of aromatic ketones (acetophenones) **2a-c** which can generate nucleophilic enolates upon treatment with a strong base. These ketones were chosen due to their relatively high acidity (pKa ~ 25) and limited bulkiness at the nucleophilic carbon center. We believed these properties would facilitate nucleophilic attack on the cyano-group of phthalonitrile, rather than the usual *ortho*-deprotonation reaction of phthalonitrile with subsequent formation of azadipyrromethene-type products.[49] Indeed, we found that a series of new (*Z*)-3-alkylidene-isoindol-1-imines **3a-c** can be easily synthesized by the reaction of phthalonitrile **1** and aromatic ketones **2a-c** in gram-scale quantities (Scheme 1).

For instance, simply mixing 4-methoxyacetophenone **2b**, phthalonitrile **1**, and potassium *tert*-butoxide in dry DMF at room temperature for 10 hours (route ***i***, Scheme 1), following by workup with aqueous ammonium chloride solution, we obtained the isoindol-1-imine derivative **3b** in 80 % yield. The scope of this reaction has been tested on other aromatic ketones **2a** and **2c**. However, it was found that under these reaction conditions the yields of target heterocycles **3a** and **3c** were quite low (6% for **3a** and 4 % for **3c**).

Scheme 1. General procedure for the synthesis of 3-alkylidene-isoindolin-1-imines 3a-c and isoindolin-1-ones 4a-c [a]

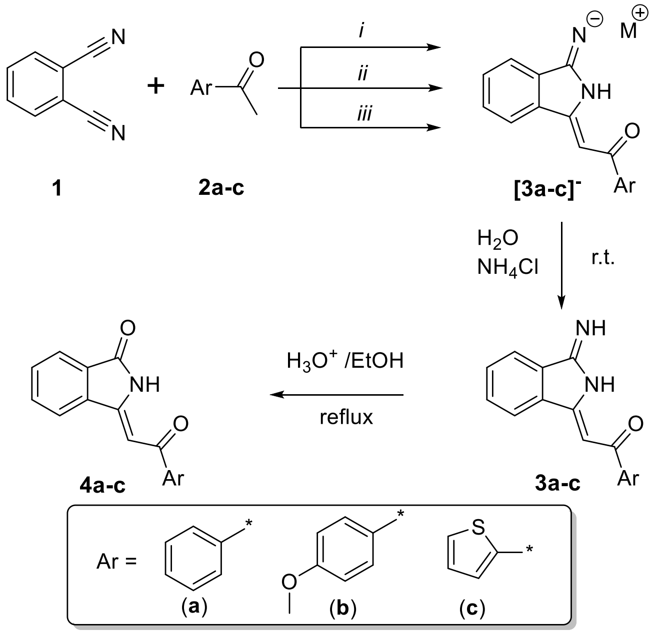

[a]Reagents and Conditions: (*i*) THF(DMF)/t-BuOK; (*ii*) DMF/NaH; (*ii*) THF/*n*-BuLi.

To improve the reaction yields, the effect of both solvent and base on the yield of 3-alkylidene-isoindol-1-imines **3a-c** was evaluated. Among different solvents examined, including THF, 1,4-dioxane, and diethyl ether, aprotic polar solvents such as dry DMF were found to be the most useful. At the same time, sodium hydride (NaH) was identified as the most suitable base for the preparation of **3a-c** (route ***ii***, Scheme 1). Surprisingly, the attempt to synthesize these compounds using lithium diisopropylamide (LDA) in THF resulted in the formation of only trace amounts of **3a-c**. The use of *n*-butyl lithium (*n*-BuLi) as a base gave a much better yields (~50 %, route ***iii***, Scheme 1). It was interesting to see, that although the reactions with both LDA and *n*-BuLi were carried out at -78 °C, the formation of phthalocyanine as a side product was detected in all cases. Thus, among three different protocols for the synthesis of heterocycles **3a-c** (THF(DMF)/t-BuOK (***i***), DMF/NaH (***ii***), and THF/*n*-BuLi (***iii***)), the combination of DMF as a solvent and NaH as a base was found to be the most successful (Scheme 1). To our surprise, no sign of the partial hydrolysis of compounds **3a-c** under aqueous workup of the reaction mixture was found, which is in a contrast to the moisture sensitivity of "half"-phthalocyanine derivatives.[27] The hydrolysis of compounds **3a-c** to products **4a-c** can be achieved by the overnight refluxing of corresponding imines in ethanol in the presence of aqueous hydrochloric acid.

^{1}H NMR spectroscopy was used in order to elucidate the stereochemistry of the imines **3a-c** (Figure 1, SI). According to the NMR data, all three compounds exist as a pure (*Z*)-isomers, which proves high stereoselectivity of this reaction. In $CDCl_3$, spectra of all three compounds contain a resonance between ~6.5 - 6.7 ppm, characteristic of the CH-singlet of the methine group located at position 3 of the isoindoline core. Compound **3a** has a broad deshielded singlet of the NH proton at 10.83 ppm, due to the formation of an intramolecular hydrogen bond between CO-group of acetophenone moiety and NH proton at position 2 of isoindoline heterocycle. This hydrogen bond is very weak and was not observed for compounds **3b** and **3c** (SI). None of the three compounds showed an imino group NH-signal at the α-position of **3a-c** in $CDCl_3$ spectra, due to fast exchange reaction with water. On the other hand, two separate broad singlets of the NH-protons at ~11 and 9 ppm can be clearly seen in DMSO-d_6 spectra for compounds **3a** and **3c** (Figure 1, SI). At the same time, DMSO-d_6 spectrum of compound **3b** has a broad singlet for two protons at 10.5 ppm, which might indicate that this molecule exists as amine-tautomer, as it was shown for another isoindoline derivative.[45]

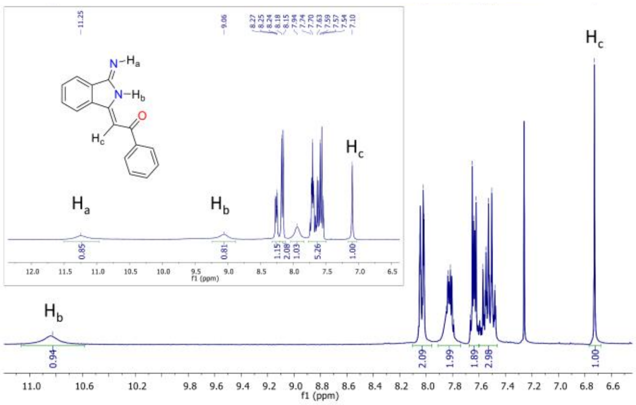

Figure 1. ^{1}H NMR spectrum of compound **3a** in $CDCl_3$ (main figure) and DMSO-d_6 (inset).

Similarly to heterocycles **3a-c**, isoindolin-1-ones **4a-c** exist in a pure (*Z*)-form at the carbon-carbon double bond, and no evidence of (*E*)-isomers was found by either NMR or X-ray analysis (Figure 2, SI). From the theoretical point of view, compounds **3a-c** can exist in four different tautomeric forms **I-IV**. Forms **III** and **IV**, however, were not observed in the NMR experiments (Chart 2).

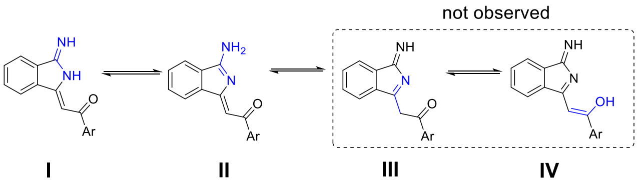

Chart 2. Plausible tautomeric forms of compounds **3a-c**.

Single-crystal X-ray diffraction studies of compounds **3b**, **3c**, and **4c** confirmed a (*Z*)-configuration at each carbon-carbon double bond, which fell within the expected C=C range in all three compounds (**3b**: 1.320(10), **3c**: 1.355(2), **4c**: 1.3500(17) Å). Similarly, short C=O bonds (**3b**: 1.235(8), **3c**: 1.240(2), **4c**: 1.2411(16) Å) and C=N (or C=O for **4c**) (**3b**: 1.264(9), **3c**: 1.276(3), **4c**: 1.2147(15) Å) bond lengths were consistent with assignment of imine tautomeric form **I** (Chart 2) for each compound.[57]

The plausible mechanism of the formation of **3a-c** is illustrated in Scheme 2 using **3b** as an example. In the first step, sodium hydride reacts with acetophenone **2b** generating nucleophilic derivative **[2b]**$^-$. This nucleophile then attacks the cyano-group of phthalonitrile **1** yielding anionic adduct **[3o]**$^-$ (open form) which undergoes intramolecular heterocyclization via another nucleophilic attack of an imine anion on the second cyano-group, producing isoindol-1-imine anionic derivative **[3b]**$^-$ (tautomer **III**). This anion tautomerizes into more stable imine form **[3b]**$^-$ (tautomer **I**) under basic reaction conditions. Finally, upon aqueous workup, this tautomer gets protonated and precipitates from the reaction mixture to give imine derivative **3b** as a pure (*Z*)-stereoisomer. We postulate that the driving force for the formation of pure (*Z*)-isomer of **3a-c** is the hydrogen bond formed between N-H and C=O fragments in **[3a-c]**$^-$.

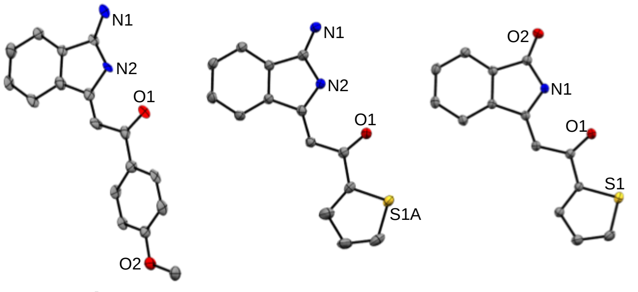

3b **3c** **4c**

Figure 2. Solid-state structures of **3b**, **3c**, and **4c** with ellipsoids shown at 50% probability levels. Hydrogen atoms and co-crystallized solvent molecules (**3b** and **3c**) are omitted for clarity.

Scheme 2. The plausible mechanism for the formation of compound 3b

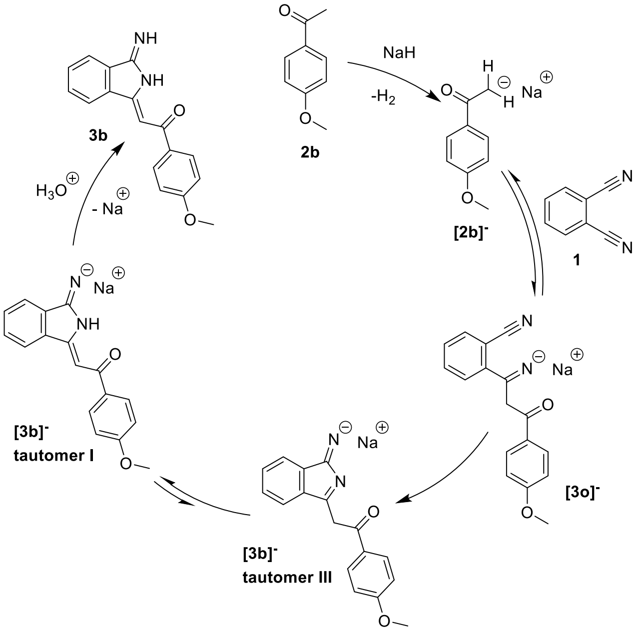

With sufficient quantities of compounds **3a-c** in hand, we decided to test their potential use as precursors for the preparation of more complex chromophores, as has been demonstrated for a number of 1,3-diiminoisoindoline derivatives,[24,31] as well as on new hybrid isoindol-1-imines (Scheme 3).[46-48] Initially, the potential for self-condensation reactions of heterocycles **3a-c**, which would give us a new class of *benzo*-fused core-extended azadipyrromethene analogs, was studied in detail. We found that under refluxing conditions for a prolonged time in non-polar solvents such as toluene or *o*-xylene, the formation of new products can be observed by the color change of the reaction mixture. Indeed, the formation of self-condensation products of compounds **3a-c** was confirmed by mass-spectrometry analysis. However, under these reaction conditions, the reaction yields of the target products were very low, and the reaction mixture was mainly consisting of the unreacted starting materials **3a-c** in all cases.

Scheme 3. Synthesis of anionic compounds $[5a\text{-}c]^-$ and their protonated derivatives 5a-c

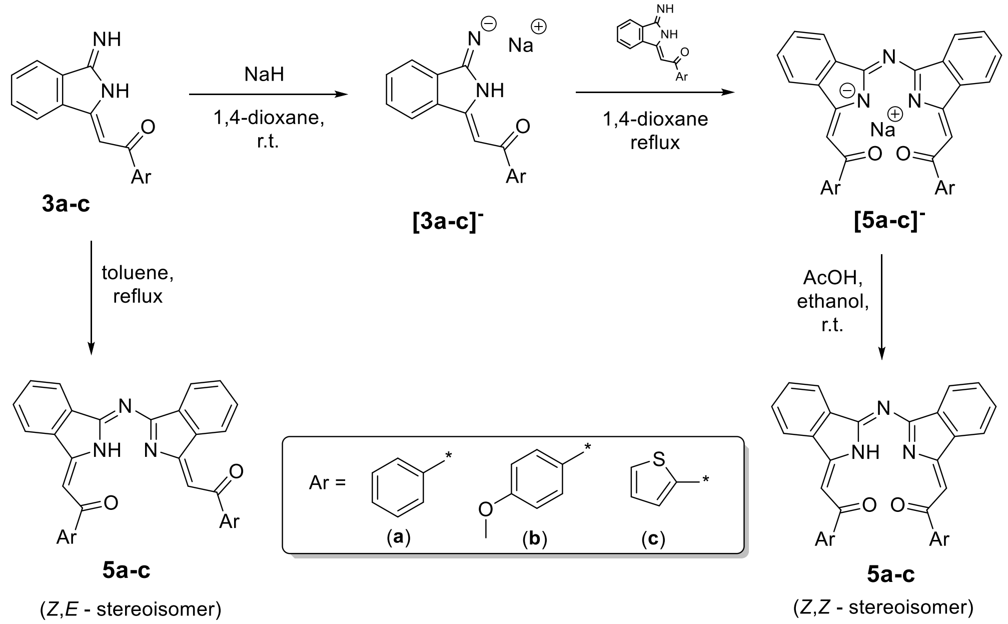

Use of other high-boiling point solvents (DMF, NMP, or quinolone) did not improve these yields. At the same time, in protic solvents such as 2-propanol, 1-butanol, or 2-dimethylamino-ethanol, no traces of desired products **5a-c** were observed even after 24 h of refluxing. Nevertheless, by refluxing isoindol-1-imine **3b** in toluene, we were able to isolate a small quantity of desired self-condensation product **5b** by column chromatography. ^{1}H NMR analysis confirmed the structure of compound **5b** and showed its unsymmetrical structure with (*Z*,*E*)-configuration at the carbon-carbon double bond at the α-position of this *benzo*-fused core-extended azadipyrromethene analog (SI Figures S19 and S20, Scheme 3). Since a simple heating approach was found to be very limited from the synthetic point of view, it was necessary to develop a new method for synthesis of desired MB-DIPY compounds **5a-c**. We thought that the deprotonated imines **[3a-c]**$^-$ would be much stronger nucleophiles compared to the parent 3-alkylidene-isoindol-1-imines **3a-c**, which might increase the overall condensation reaction rate. Indeed, it was found that the reaction between **3a-c** and their sodium salts **[3a-c]**$^-$ (prepared by the deprotonation of **3a-c** with sodium hydride) in 1:1 molar ratio under the refluxing conditions in dry 1,4-dioxane leads to the formation of desired condensation MB-DIPY products **[5a-c]**$^-$ in almost quantitative yields. Although the anions **[3a-c]**$^-$ are stable enough for isolation and characterization, they were used for the condensation with another equivalent of appropriate isoindoline **3a-c** *in situ*. This reaction is very sensitive to moisture, thus the use of a dry solvent, as well as inert atmosphere, is optimal. Since compounds **[5a-c]**$^-$ are not stable for TLC analysis, reaction progress was monitored by UV-Vis spectroscopy. After two hours of the refluxing an intense purple solution was formed in all cases. After cooling to room temperature, the reaction products **[5a-c]**$^-$ can be easily precipitated from the reaction mixture by the addition of *n*-hexane. In the solid-state, MB-DIPYs **[5a-c]**$^-$ were found to be quite stable, and can be stored at ambient conditions for a long time. The formation of anionic dyes **[5a-c]**$^-$ was first confirmed by the NMR spectroscopy (Figure 3, SI). The solubility of these compounds in $CDCl_3$ was found to be low and the slow fading of the intense purple color was observed while using this solvent. In the case of highly polar DMSO-d_6, slow degradation of these compounds was observed as well. Thus, the NMR spectra on anionic compounds **[5a-c]**$^-$ were recorded using dry acetone-d_6 as the solvent, due to a good solubility and stability of these dyes in this media.

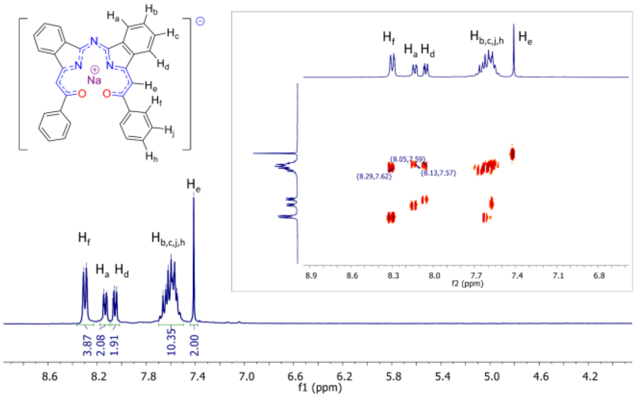

Figure 3. ^{1}H- and ^{1}H-^{1}H COSY (inset) NMR spectrum of compound **[5a]**$^-$ in $(CD_3)_2CO$-d_6

Similar to isoindol-1-imines **3a-c**, the NMR spectra of MB-DIPYs **[5a-c]**$^-$ have a characteristic CH-singlet of the methine group at α-position observed around 7.5 ppm. Unlike the thermal self-condensation reaction, the reaction with the sodium ion as a template allows for very high product yields. More importantly, the NMR spectra of anionic compounds **[5a-c]**$^-$ indicate their symmetric structure with (*Z*,*Z*)-configuration at the carbon-carbon double bond (Figure 3, SI Figures S21 – S29).

Scheme 4. Synthesis of compounds 7a-c and 8a-c.

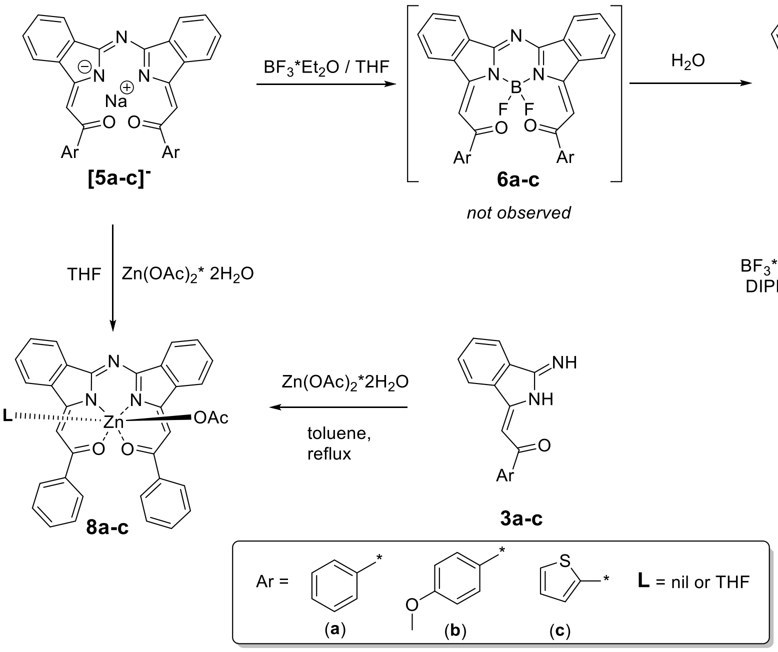

The template chelation of sodium cation by the N_2O_2 coordination sphere during the condensation reaction allows retention of this configuration even under refluxing conditions in 1,4-dioxane. Thus, sodium hydride serves not only as a base for the deprotonation of starting isoindol-1-imines **3a-c** but also as a template during the self-condensation reaction, which is the key for the stereoselective preparation of (*Z,Z*)-isomers of **[5a-c]**$^-$. The role of the template can be also confirmed by the X-ray structure of **[5c]**$^-$, in which sodium counter-ion is chelated by the anionic ligand (Figure 4), which further dimerizes in the solid-state *via* intermolecular Na-N(aza) interactions that are slightly longer (2.7070(14), 2.8865(14) Å; two crystallographically distinct molecules in the asymmetric unit; SI) compared with the two intramolecular Na-N distances.

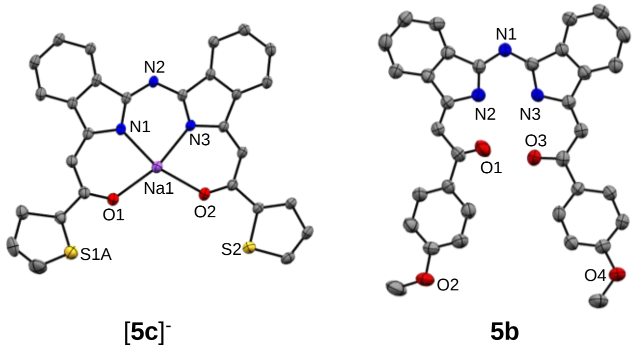

Figure 4. Solid-state diagrams of MB-DIPYs **[5c]**$^-$ and **5b** with ellipsoids shown at 50% probability levels. Hydrogen atoms and the second half of symmetry-generated dimeric unit of **[5c]**$^-$ are omitted for clarity. For **[5c]**$^-$, one of two unique molecules in asymmetric unit is shown.

We thought that simple treatment of MB-DIPYs **[5a-c]**$^-$ with acid following by the liquid-liquid extraction with organic solvent would give us the protonated dyes **5a-c**. However, this was not the case. Instead, treatment of **[5a-c]**$^-$ with Brönsted acids leads to an immediate change of intense purple color to a less intense yellow solution, and after the workup of the reaction mixture, the only trace amounts of desired dyes **5a-c** were found by the NMR analyses. Evidently, these compounds undergo partial hydrolysis in aqueous solution, which minimizes the total yield of the metal-free MB-DIPYs **5a-c**. The presence of hydrolysis products **3a-c** can also be seen from the TLC analysis of the reaction mixture. This observation forced us to synthesize compounds **5a-c** by the addition of a small excess of acetic acid into the suspension of appropriate anionic dyes **[5a-c]**$^-$ in alcohol in 50 - 60 % yield. The target protonated products precipitate from the ethanol solution as a fine brown powder, which can be collected by vacuum filtration. The symmetric structure of these compounds was confirmed by ^{1}H NMR analyses as well as X-ray crystallography in the case of compound **5b** (Figure 4). The characteristic NH peak around 13 ppm can be clearly seen in their ^{1}H NMR spectra (SI Figures S30 - S38). Also, similar to the anionic dyes **[5a-c]**$^-$, all protonated dyes **5a-c** retain a (*Z,Z*)-configuration at the carbon-carbon double bond.

It is well known from the chemistry of BODIPYs and aza-BODIPYs that the formation of a rigid six-membered ring by chelation of dipyrromethenes or azadipyrromethenes with BF_2 fragment leads to a significant redshift of both absorption and emission spectra.[58-60] From X-ray data and DFT calculations, it was clear for us that the N_2O_2 cavity in MB-DIPYs **[5a-c]**$^-$ is likely too small to fit the entire BF_2 fragment. Nevertheless, this reaction has been tested by the addition of boron trifluoride etherate solution to **[5a-c]**$^-$ in THF to see if BF_2-coordination of the boron center into N_2O_2 cavity will occur. After the aqueous solution workup of the reaction mixture, the TLC analysis showed the formation of a small amount of highly fluorescent product in all cases. The products **7a-c** were purified by chromatography and analyzed by proton NMR (SI Figures S39 – S41). It was found, that these fluorescent dyes are BF_2-complexes of isoidolin-1-ones **4a-c**, which are the hydrolysis products of **[5a-c]**$^-$. Dyes **7a-c** can also be obtained by the direct synthesis starting from compounds **4a-c** in a very high reaction yields (Scheme 4). In addition to the spectroscopic methods, the

X-ray crystallography on **7b** (Figure 5) confirms successful coordination of the BF_2 fragment by isoindolic nitrogen and C=O group oxygen atoms.

A nearly square-planar geometry of the N_2O_2 cavity in MB-DIPYs **[5a-c]**$^-$, on the other hand, can be potentially used as a platform for synthesis of main-group and transition-metal complexes. Indeed, a simple treatment of the THF solutions of anionic dyes **[5a-c]**$^-$ with a stoichiometric amount of zinc(II) acetate leads to the formation of a series of zinc complexes **8a-c** in high yield (Scheme 4). Unlike sodium salts **[5a-c]**$^-$, MB-DIPYs **8a-c** are chemically stable and do not undergo the hydrolysis in the presence of usual protic solvents. Although complexes **8a-c** have very low solubility, their structure can be confirmed by ^1H NMR (SI Figures S42 – S44) and high-resolution mass spectroscopy (SI Figures S67 – S69). The presence of both acetate and THF signals in their ^1H NMR spectra is indicative of the formation of hexacoordinated rather than pentacoordinated compounds. Crystals of **8c** suitable for the X-ray analysis were obtained by slow diffusion of acetonitrile into an acetic acid solution of the MB-DIPY (Figure 5). The Zn(II) center in **8c** has a similar N_2O_2 coordination environment to the sodium cation in **[5c]**$^-$, but is capped instead by an acetate anion in axial position. The Zn bears a τ_5 parameter consistent with distorted square pyramidal geometry (0.09), where the Zn is pushed out of the N_2O_2 plane (two largest angles are N(2)-Zn(1)-O(2) 156.32(10)° and N(3)-Zn(1)-O(1) 151.01(10)°).

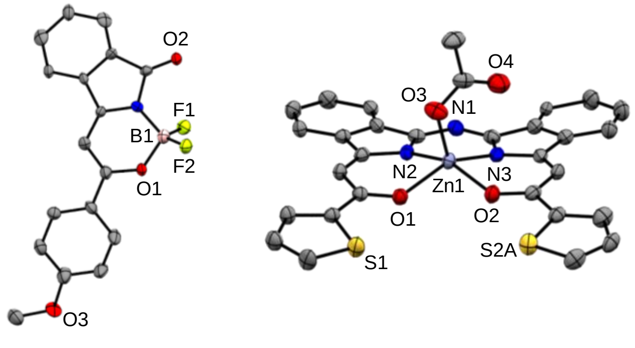

7b **8c**

Figure 5. Solid-state diagrams of **7b** and **8c** with ellipsoids shown at 50% probability levels. Hydrogen atoms and co-crystallized solvent molecules (**8c**) are omitted for clarity. For **7b**, one of two unique molecules in asymmetric unit is shown.

Attempts for the preparation of reduced *B,O*-chelated aza-BODIPYs.

Despite the substantial similarity with the traditional azadipyrromethene chromophores, the new core-extended MB-DIPYs **5a-c**, **[5a-c]**$^-$, as well as their zinc complexes **8a-c** represent a completely different and novel class of compounds. Indeed, these molecules can be considered as the two-electron oxidized cores of *benzo*-fused azadipyrromethenes **9a-c** (Scheme 5). Thus, the potential two-electron reduction followed by the proton transfer reaction in these highly electron-deficient systems might result in the formation of a regular core-extended azadipyrromethenes and corresponding main-group and transition-metal complexes.

To probe new MB-DIPY chromophores toward chemical reduction, a variety of reducing agents (H_2/Pd(C), $NaBH_4$, $LiAlH_4$, and $NaBH_3CN$) have been tested out on these systems. Similar to Cammidge and coworkers' report on related core-modified aza-BODIPY analogs,[46] no sign of the formation of desired reduction products was observed. For instance, the reduction of new chromophores with hydrogen gas in the presence of Pd/C catalysis leads to the formation of colorless products. In the case of strongly basic reducing agents as $NaBH_4$ and $LiAlH_4$ the formation of anionic MB-DIPYs **[5a-c]**$^-$ were observed.

Scheme 5. The theoretical two-electron reduction process of compounds 5a-c.

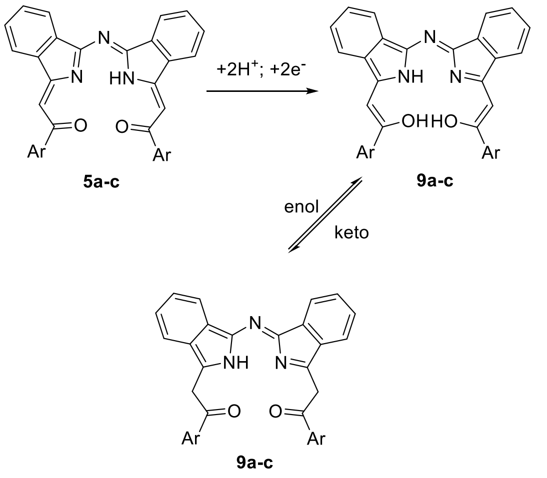

Based on these preliminary observations, we thought, that the use of a weakly basic reducing agent such as $NaBH(OAc)_3$ (sodium triacetoxyborohydride, STAB) might avoid the undesirable deprotonation reaction and will lead to the formation of the target reduction products. Indeed, when STAB was used as a reducing agent, the formation of a deeply colored brown solution was observed while heating of the toluene solution of **5a** with a small excess of reducing agent (Scheme 6).

Scheme 6. The synthesis of compounds 10a-c and their *B,O*-chelated derivatives 11a-c under two-electron reduction process of 5a-c with STAB.

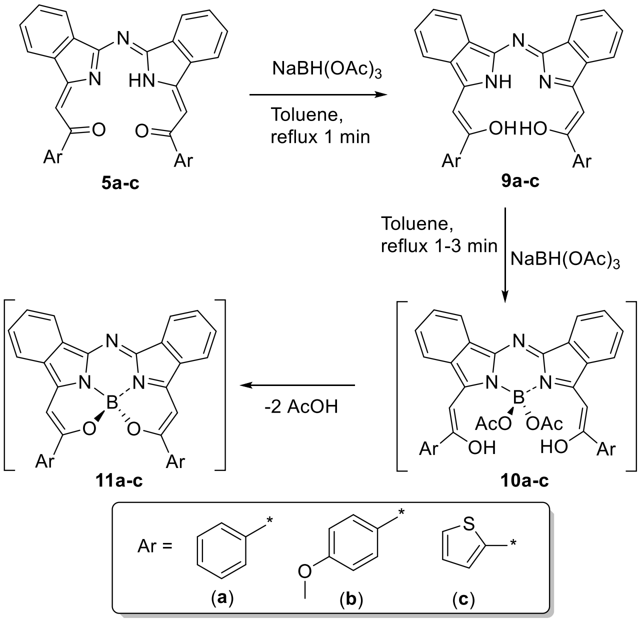

The scope of this reaction was tested on compounds **5a-c**. It was found, that the reduction products are not stable and quickly decompose under the reaction mixture workup conditions even under the inert gas atmosphere. A new reduced systems **11a-c**, however, were found to be stable enough for characterization by UV-Vis and high-resolution mass spectroscopy. According to the HRMS analysis (Figure 6, SI Figures S70 – S75), these molecules are present as *B*,*O*-chelated aza-BODIPYs **11a-c**, which are the products of boron chelation of dyes **9a-c**. Also, the molecular peaks of the corresponding non-chelated intermediate compounds **10a-c** can be found in their mass spectra.

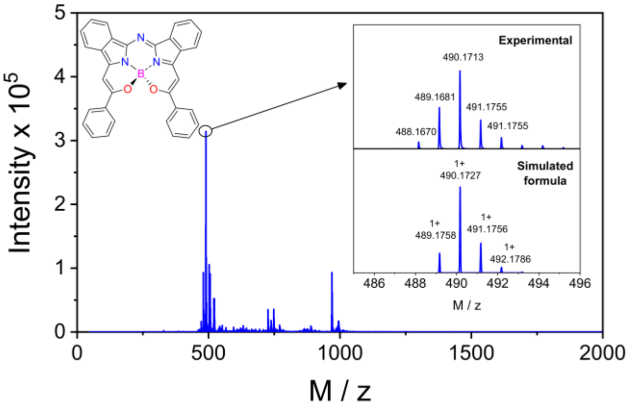

Figure 6. APCI high-resolution mass spectrum of compound **11a.**

Absorption and emission spectra.

All new compounds were characterized by the UV-Vis and fluorescence spectroscopy (Table 1, Figures 7 and 8, and SI Figures S76 – S89). The anionic MB-DIPYs **[5a-c]**$^-$ have very similar absorption profiles with three major absorption peaks observed around 580, 545 and 360 nm (Figure 7). The higher-energy transition observed around 360 nm show the highest molar extinction coefficients in an order of 35,000 M^{-1} cm^{-1}, whereas the lowest-energy transitions (~580 nm) were found to be less intense (ε ~20,000 M^{-1} cm^{-1}). Experimental molar extinction coefficients for anionic **[5a-c]**$^-$ are significantly lower compared to the classic aza-BODIPY and aza-DIPY systems.[61-63] The absorption shoulder observed at ~545 nm was assigned as the vibronic satellite of the first excited state (Figure 7). MB-DIPYs **[5a-c]**$^-$ are highly emissive and show the emission maximum around 600 nm with a shoulder at 650 nm (Table 1). The emission profiles look close to the mirror images of the corresponding absorption spectra (SI Figures S76 – S78) and are indicative of relatively small (~20 nm) Stokes shifts that are reflective of rather small geometry reorganization of the first excited state of these systems. Because of the low stability of diluted solutions of MB-DIPYs **[5a-c]**$^-$ toward hydrolysis, their quantitative fluorescence quantum yields were not determined.

In general, the absorption profiles of zinc MB-DIPYs **8a-c** are very similar to those of **[5a-c]**$^-$. However, the lowest-energy transitions are less intense (ε ~15,000 M^{-1} cm^{-1}) and slightly (~15 nm) blue-shifted compared to **[5a-c]**$^-$. Although the excitation spectra of **8a-c** closely resembled their absorption spectra (SI Figures S99 – S101), the fluorescence spectra of these compounds are not the mirror images of the excitations spectra and are dominated by a peak around 610 nm, followed by a shoulder of smaller intensity (Figure 7). The solutions of MB-DIPYs **8a-c** look less fluorescent compared to **[5a-c]**$^-$ to the naked eye, with fluorescence quantum yields of ~10 % (Table 1). It should be mentioned, that the aromatic group adjacent to the carbonyl of dyes **[5a-c]**$^-$ and **8a-c** has a minor impact on the absorption and fluorescence spectra. Indeed, in the case of thiophene derivatives, the small redshift (~10 nm) was observed in both absorption and emission spectra. Also, the lowest-energy transitions in the dyes **[5c]**$^-$ and **8c** are more intense, compared to those of phenyl- and *p*-methoxyphenyl-substituted compounds. Apparently, this is due to a better degree of conjugation of five-membered thiophene ring compared to the six-membered phenyl groups.

In contrast to anionic **[5a-c]**$^-$ and zinc complexes **8a-c**, the protonation of **[5a-c]**$^-$ leads to a drastic change in their absorption profiles (Figure 8). Indeed, upon the treatment of **[5a-c]**$^-$ with the acid, these deeply colored and fluorescent purple compounds transform into yellow-brownish weakly colored solutions. The absorption spectra of MB-DIPYs **5a-c** are, in general, very similar to those azadipyrromethene-analogs described by Cammidge and coworkers.[48] These compounds display an intense absorption in a UV-region around 330 nm, the less intensive and broad peaks around 450 nm, as well as a very weak low-energy transition around 580 nm.

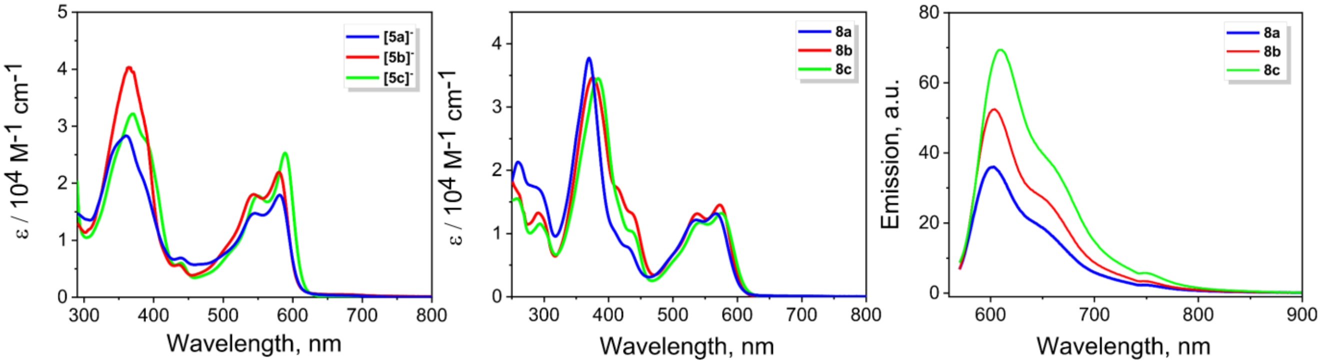

Figure 7. UV-Vis absorption spectra of MB-DIPYs **[5a-c]**$^-$ in THF (left), **8a-c** in DCM (middle), and fluorescence spectra of **8a-c** in DCM solution (right).

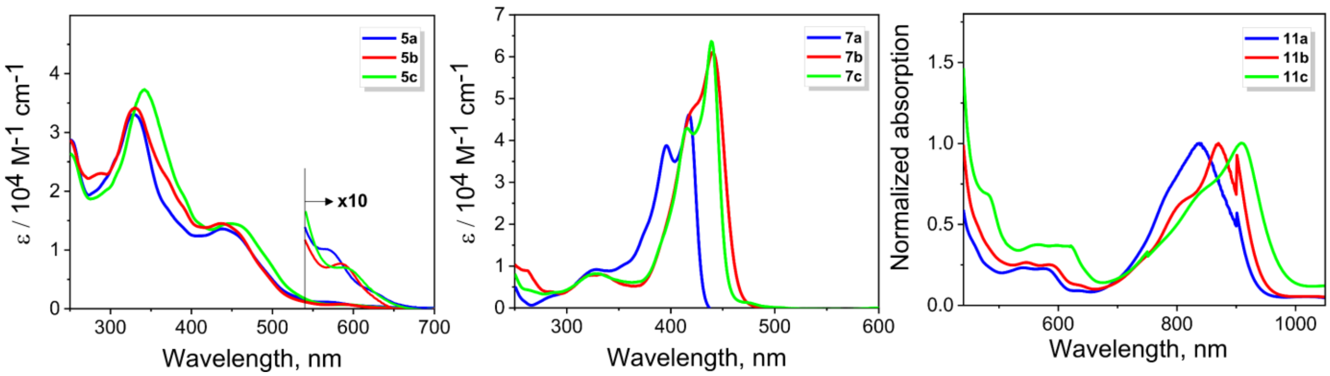

Figure 8. UV-Vis absorption spectra of MB-DIPYs **5a-c** (left), **7a-c** (middle) in DCM and **11a-c** in toluene (right).

MB-DIPYs **5a-c** were found to be weakly fluorescent with the emission maxima around 600 nm and fluorescent quantum yields between 5 and 7% (Table 1). Such drastic changes in both absorption and emission spectra are the result of more flexible geometries of protonated MB-DIPYs **5a-c** compared to the rigidified structures of **[5a-c]**$^-$ and **8a-c**.

The UV-Vis spectra of BF$_2$-containing systems **7a-c** resemble those of classic BODIPYs[8-12] and BOPHYs[19,21-23] with the strong absorption band centered between 420 and 440 nm, which is followed by a set of much less intense transitions between 250 and 400 nm (Figure 8). Compounds **7a-c** are fluorescent (Table 1) with their fluorescence spectra being close to the absorption mirror images (SI Figures S82 – S84). The excitation spectra of all fluorescence compounds shown in the Supporting Information. Except the metal-free compounds **5a-c**, the excitation spectra are close to the respective absorption spectra. In case of the metal-free compounds **5a-c**, the excitation spectra are closer to those observed for the zinc complexes **8a-c** and this discrepancy will be further probes by the time-resolved spectroscopic methods.

The chemical reduction of MB-DIPYs **5a-c** (Scheme 6) allowed us to transform these chromophoric systems into the classical *B,O*-chelated aza-BODIPY systems **11a-c**. The treatment of protonated systems **5a-c** with STAB in refluxing toluene resulted in the formation of deeply colored brown (**11a**) to green (**11c**) solutions. As it was mentioned above, these systems were found to be not stable in solution. However, their UV-Vis-NIR spectra can be collected by the immediate recording after the reduction reaction. The normalized absorption spectra on the reduced species **11a-c** are shown in Figure 8. The *B,O*-chelated dyes exhibit NIR absorption with the maxima at 840, 870, and 910 nm for **11a**, **11b**, and **11c** respectively. The fluorescence measurements of these dyes were not conducted, due to their low stability.

Table 1. Spectroscopic properties of the dyes presented in this report.

Compound	λ_{abs}., nm ($\varepsilon \cdot 10^{-3}$, M$^{-1}\cdot$cm^{-1})	λ_{em}, nm (Φ_F)	Stokes shift, cm^{-1}
[5a]$^-$ [a]	581 (17.9), 546 (14.7), 360 (28.2)	604	655
[5b]$^-$ [a]	580 (21.9), 544 (18.0), 364 (40.2)	600	575
[5c]$^-$ [a]	589 (25.3), 550 (17.7), 371 (32.1)	608	530
5a	577 (1.1), 440 (13.0), 330 (33.0)	613 (0.07)	1018
5b	581 (0.7), 437 (14.5), 330 (34.1)	606 (0.07)	710
5c	590 (0.6), 446 (14.0), 342 (37.2)	615 (0.05)	689
7a	418 (46.1)	430 (0.03)	668
7b	440 (61.0)	473 (0.27)	1586
7c	439 (63.6)	451 (0.12)	607
8a [a]	565 (13.1), 536 (12.1), 370 (37.6)	603 (0.07)	1116
8b [a]	573 (14.5), 538 (13.1), 375 (34.5)	604 (0.13)	896
8c [a]	575 (13.2), 542 (11.7), 384 (34.5)	609 (0.10)	971
[8a]$^{\cdot-}$	1190, 1034, 720, 638, 588, 480, 399	-	-
[8b]$^{\cdot-}$	1186, 1030, 717, 642, 589, 480, 402	-	-
[8c]$^{\cdot-}$	1236, 1068, 740, 646, 592, 490, 408	-	-
11a [b]	840	-	-
11b [b]	870	-	-
11c [b]	910	-	-
[12a]$^-$ [a,b]	720, 680, 400, 335	753	608
[12b]$^-$ [a,b]	71 2, 664, 439, 388, 336	750	711
[12c]$^-$ [a,b]	730, 696, 448, 403, 335	763	592

[a] Spectroscopic measurements were done in dry THF

[b] Compounds are not stable in solution for a prolonged time

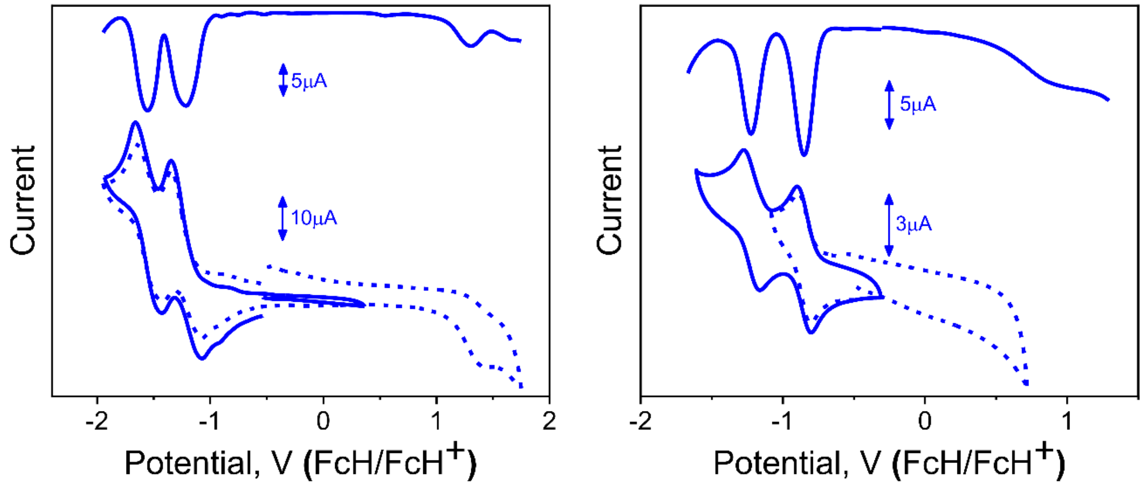

Figure 9. CV (bottom) and DPV (top) spectra of MB-DIPYs **5a** (left) and **8a** (right) in deoxygenated 0.1 M TBAP/DCM system.

Electrochemical and spectroelectrochemical studies

The redox properties of the MB-DIPYs **5a-c**, as well as their zinc(II) complexes **8a-c**, were probed by cyclic voltammetry (CV), and differential pulse voltammetry (DPV) techniques. All experiments were done in deoxygenated 0.1 M TBAP (tetrabutylammonium perchlorate) DCM solutions. In the case of protonated dyes **5a-c** two fully reversible reduction processes separated by ~300 mV can be observed in both CV and DPV at ~ -1.2 V and ~ -1.5 V (Figure 9, Table 2, and SI Figures S102, S103). Despite the highly electron-deficient properties of these compounds, their irreversible oxidation can be observed around +1.3 V, which is anodically shifted compared to classical dipyrromethene systems.[64-66] On the other hand, zinc(II) complexes **8a-c** are even more electron-deficient systems according to CV and DPV data. The first reduction potentials of these complexes are anodically shifted by ~350 mV compared to protonated species **5a-c** (-0.85 V for compounds **8a** and **8c** and -0.95 V for **8b**). Such low reduction potentials are comparable with those observed for C_{60} fullerene and its derivatives (~ -1.1 V),[67-69] which makes zinc MB-DIPYs complexes **8a-c** good candidates for non-fullerene acceptors in organic heterojunction solar cells. The second reductions are also reversible and anodically shifted by ~300 mV compared to **5a-c**. The oxidation peaks were not detected within the electrochemical window for zinc complexes although small, diffuse peak was observed in their DPV curves at ~+0.8V (Figure 9, S104, S103).

Table 2. Redox properties of compounds 5a-c and 8a-c in 0.1 M TBAP DCM solutions. [a]

Compound	Ox., V	Red. 1, V	Red. 2, V
5a	1.30 [b]	-1.21	-1.51
5b	1.36 [b]	-1.26	-1.54
5c	1.38 [b]	-1.16	-1.39
8a	-	-0.85	-1.23
8b	-	-0.95	-1.29
8c	-	-0.85	-1.21

[a] All potentials are referenced to the FcH/FcH$^+$ couple; Scan rate – 100 mV/s;

[b] – irreversible process

To probe the electron-accepting properties of zinc complexes, we conducted spectroelectrochemical experiments on MB-DIPYs **8a-c**. It was found that during the first reduction process in these compounds under the spectroelectrochemical conditions, the decrease of π- π^* transition around 570 nm and the formation of two peaks at 490 and 660 nm occurred in all cases. In addition, two new quite intense NIR peaks at ~1000 and ~1250 nm were observed, which is indicative of the formation of paramagnetic open-shell anion-radical species **[8a-c]**$^{\cdot-}$. The second reduction can be also successfully followed by spectroelectrochemical approach. During the second reduction, the decrease of NIR peaks at ~1000 and ~1250 nm and the formation of a peak at 700 nm were observed for all compounds. This peak is accompanied by a vibronic satellite and is energetically close to the main low-energy transition observed in the case of nickel azadipyrromethene N_2O_2 complex reported by us earlier.[55] Thus, we have tentatively assigned this transition to the fingerprint band of desired two-electron reduced closed-shell *benzo*-fused zinc azadipyrromethenes **[12a-c]**$^-$ (Scheme 7).

Stepwise one- and two-electron reductions of zinc complexes **8a-c** can be achieved not only under spectroelectrochemical conditions but also by the direct chemical reduction with $NaBH_4$ (Scheme 7). It was found that upon the treatment of THF suspensions of **8a-c** with $NaBH_4$, under the inert gas atmosphere, the formation of deep-green colored solution (similar to that observed in spectroelectrochemical experiments) can be observed in all cases. The UV-Vis-NIR analysis on these solutions is suggestive of the formation of one-electron reduced open-shell species **[8a-c]**$^{\cdot-}$ with the characteristic NIR absorption around 1200 nm for all three compounds. Expectedly, NMR spectra of these one-electron reduced species are paramagnetic (SI Figure S45). In general, the absorption profiles of chemically generated anion-radicals are very close to each other and are in a good agreement with spectroscopic signatures observed in spectroelectrochemical experiments (Figure 10, SI Figures S106 – S110).

The open-shell species **[8a-c]**$^{\cdot-}$ were found to be moderately stable under ambient atmosphere, and their oxidation into the starting, red-colored MB-DIPYs **8a-c**, was observed after ~30 min. The further reduction of these compounds into the two-electron-reduced species **[12a-c]**$^-$ can be achieved by the addition of tetramethylammonium hydroxide, which stabilizes these systems by tetramethylammonium counter-ion.

Scheme 7. Stepwise chemical one- and two-electron reductions of MB-DIPYs 8a-c.

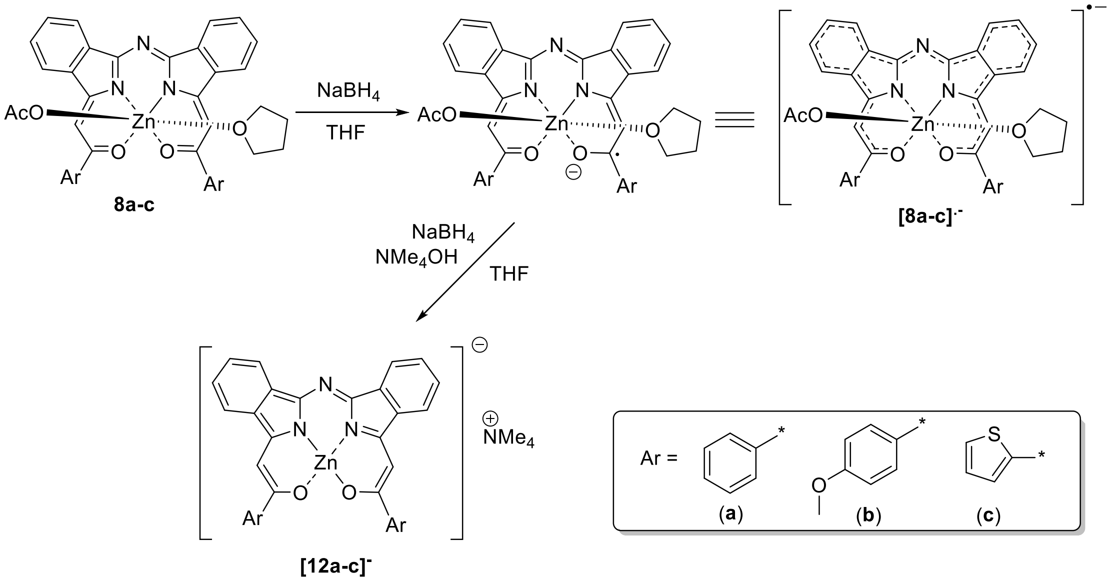

Closed-shell diamagnetic systems **[12a-c]**$^-$ display the absorption around 740 nm, which is about 160 nm redshifted compared to starting **8a-c**. Their closed-shell electronic structure can be also confirmed by fluorescence and ^{1}H NMR spectroscopy (SI Figure S46). Indeed, all three reduced derivatives **[12a-c]**$^-$ were found to be fluorescent and show the emission maxima around 755 nm (Table 1, SI Figures S85 – S87). Despite their stabilization by tetramethylammonium cation, fully reduced species **[12a-c]**$^-$ are not stable enough for large-scale isolation using conventional synthetic methods. They are, however, can be re-oxidized back to the zinc MB-DIPYs **8a-c** in the oxygen atmosphere after the addition of acetic acid.

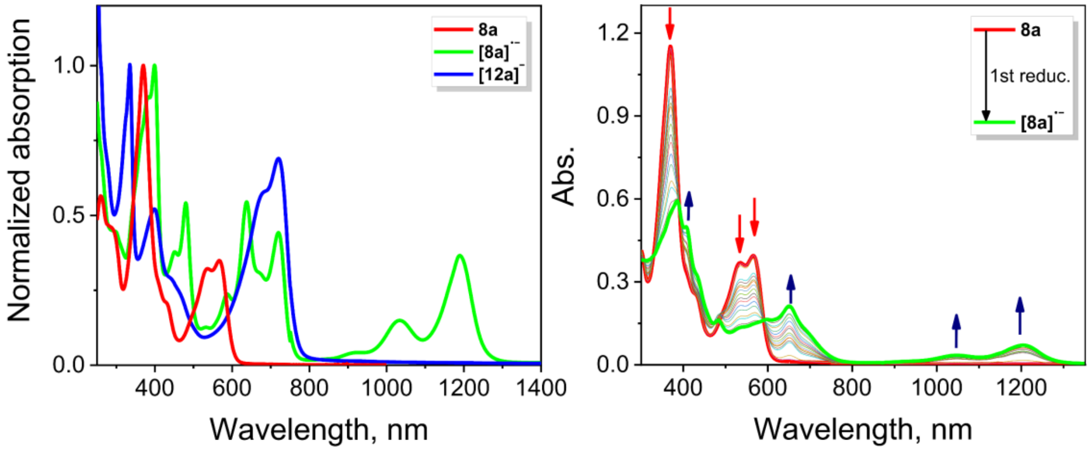

Figure 10. UV-Vis-NIR absorption spectra of MB-DIPY **8a** (red) and its one-electron-reduced **[8a]**$^{\bullet-}$ (green) and two-electron-reduced **[12a]**$^-$ (blue) derivatives obtained by the reduction with NaBH$_4$ in THF (left) and **8a**→ **[8a]**$^{\bullet-}$ transformation under spectroelectrochemical reduction conditions in deoxygenated 0.3 M TBAP/DCM system (right).

Quantum-chemical calculations

To gain insight into the photophysical and electrochemical properties of the electron-deficient MB-DIPYs **[5a-c]**$^-$, **5a-c**, and **8a-c** as well as their reduced derivatives **11a-c** and **[12a-c]**$^-$, we have conducted DFT and TDDFT calculations on these systems. The molecular orbital energy diagram of **[5a-c]**$^-$, **5a-c**, and **8a-c** is presented in Figure 11. In the case of anionic dyes **[5a-c]**$^-$ and their zinc complexes **8a-c**, the predicted energies for the HOMOs are close to each other in all systems, while the energies of LUMOs in **8a-c** are lower, which is in a good agreement with their experimental absorption spectra and redox potentials. A similar trend can be observed for the protonated dyes **5a-c**, however, the HOMOs are slightly more stabilized while the LUMO energies remain the same. These differences in the electronic structure lead to the higher HOMO-LUMO energy gap, which results in a blue shift of their absorption bands.

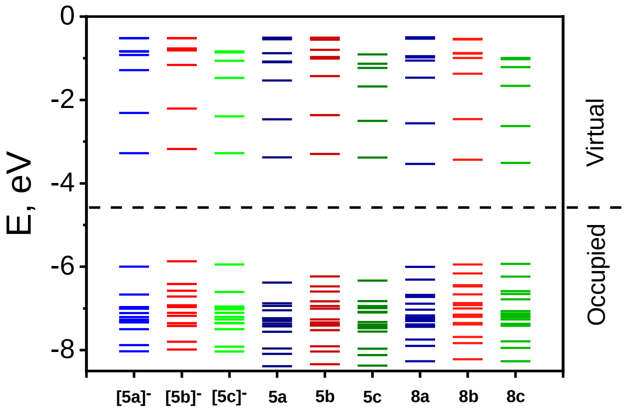

Figure 11. DFT-predicted molecular energy diagram of MB-DIPYs **[5a-c]**$^-$, **5a-c**, and **8a-c**.

It is worth mention that in the case of *p*-methoxy-substituted dyes **[5b]**$^-$, **5b**, and **8b**, the LUMOs are slightly destabilized compared to the phenyl- or thiophene-substituted dyes. This correlates well with their CV and DPV data, in which the reduction potentials of these systems are anodically shifted. The frontier molecular orbitals of the **[5a]**$^-$, **5a**, and **8a** systems are presented in Figure 12 and their compositions described in the SI.

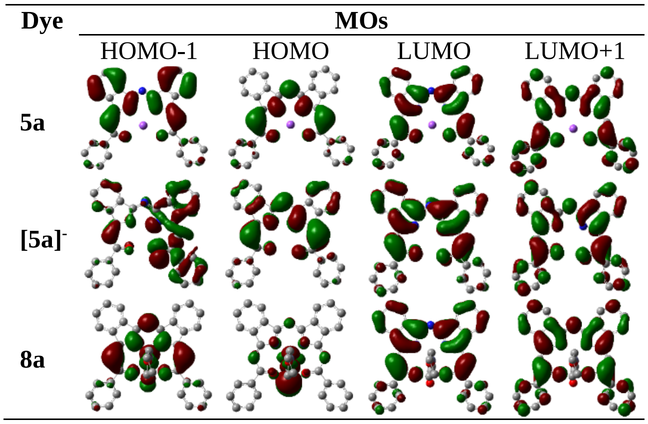

Figure 12. DFT-predicted frontier orbitals of MB-DIPYs **[5a]**$^-$, **5a**, and **8a**.

When compared to the regular BODIPYs and aza-BODIPYs, the DFT-predicted frontier π-orbitals of compounds **[5a-c]**$^-$, **5a-c**, and **8a-c** were found to be flipped. Indeed, in the case of the regular BODIPYs and aza-BODIPYs,[70-72] the HOMO resembles "half" of the classic porphyrin a_{1u} orbital with a large contribution from the pyrrolic α- and β-carbon atoms, while the LUMO resembles a "half" of the classic porphyrin a_{2u} orbital that is dominated by the contribution from the pyrrolic nitrogen atoms and the *meso*-carbon or nitrogen atom. In the case of MB-DIPYs **[5a-c]**$^-$, **5a-c**, and **8a-c**, DFT predicts that the highest energy π-centered orbital has a large contribution from the nitrogen atoms complemented by the significant contribution from the carbonyl groups. In addition, in the case of thiophene- and *p*-methoxyphenyl substituted systems, this orbital also has a significant contribution from these aromatic substituents, while such contribution from the phenyl fragment is much smaller (SI). The HOMOs in MB-DIPYs **[5a-c]**$^-$, **5a-c**, and **8a-c** resemble the LUMO is regular BODIPYs and aza-BODIPYs. The DFT-predicted LUMOs in compounds **[5a-c]**$^-$, **5a-c**, and **8a-c** have a significant contribution from the pyrrolic α- and β-carbon atoms complemented by a contribution from the carbonyl groups and, to a lesser extent, peripheral aromatic groups (SI). Again, such electron distribution resembles the HOMO of regular BODIPYs and aza-BODIPYs. Importantly, the DFT-predicted LUMO+1s in compounds **[5a-c]**$^-$, **5a-c**, and **8a-c** again have a large contribution from the nitrogen atoms similar to the LUMOs in classic BODIPYs and aza-BODIPYs. Thus, we reasoned that the two-electron reduction of compounds **[5a-c]**$^-$, **5a-c**, and **8a-c** should result in the typical for BODIPYs and aza-BODIPYs electronic structure, with electronic spectra which agree with experimental observations and DFT/TDDFT predictions as discussed below.

Although UV-Vis spectra of the MB-DIPYs **[5a-c]**$^-$, **5a-c**, and **8a-c** are somewhat different, TDDFT calculations (Figure 13) suggest that the similar excited states contribute the most into their spectroscopic signatures. In the case of sodium salts **[5a-c]**$^-$, TDDFT calculations predicted that their UV-Vis spectra are dominated by three excited states. The first, lowest energy intense band observed for all three compounds between 550 and 600 nm originates from the HOMO → LUMO single-electron excitation, the lower intensity band observed around 420 nm is dominated by the HOMO-1 → LUMO single-electron excitation, and the most intense band observed between 360 and 380 nm is dominated by the HOMO → LUMO+1 single-electron excitation. In addition, TDDFT calculations correctly predicted low-energy shift for the lowest energy transition going from **[5a]**$^-$ to **[5b]**$^-$ to **[5c]**$^-$. In the case of zinc complexes **8a-c**, the DFT-predicted HOMO is localized over the axial acetate group. It was therefore unsurprising to see that the low-energy acetate-to-chromophore charge-transfer transition was predicted by TDDFT calculations between 635 and 667 nm. The TDDFT-predicted intensity of such CT band is rather small, explaining why it was not observed in the experimental spectra. Similar to the anionic MB-DIPYs **[5a-c]**$^-$, the most intense, low-energy band observed experimentally between 565 and 575 nm for **8a-c** is dominated by the highest energy, chromophore-centered HOMO-1 to LUMO single-electron excitation. Again, TDDFT calculations correctly predicted a low-energy shift of this band going from **8a** to **8b** to **8c**. In addition, TDDFT calculations have also predicted several excited states around 500 nm, which are, probably, responsible for the absorption between 470 and 520 nm observed experimentally. As in the case of sodium salts, the most intense transition in the 360-380 nm region is dominated by the HOMO-1 → LUMO+1 single-electron excitation. In the case of protonated compounds **5a-c**, TDDFT correctly predicted that the most intense low-energy band experimentally observed between 420 and 440 nm should be shifted to the higher energy compared to the other systems. Similar to sodium and zinc compounds, it is still dominated by the HOMO → LUMO single-electron transition, while the most intense band observed between 320 and 350 nm is dominated by the HOMO → LUMO+1 single-electron excitation. Finally, similarly to the regular BF$_2$-coordinated chromophores (BODIPYs, aza-BODIPYs, and BOPHYs), TDDFT calculations predict that the HOMO → LUMO single-electron excitation is responsible for the strongest absorption band observed between 420 and 440 nm in BF$_2$-coordinated compounds **7a-c** (SI Figures S120-S122).

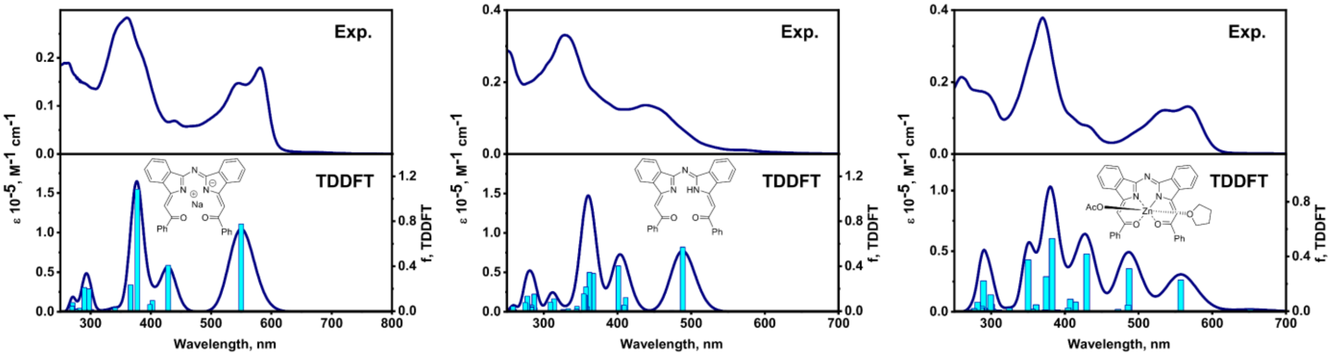

Figure 13. TD DFT-predicted electronic spectra of MB-DIPYs **[5a]**$^{-}$ (left), **5a** (middle), and zinc complex **8a** (right)

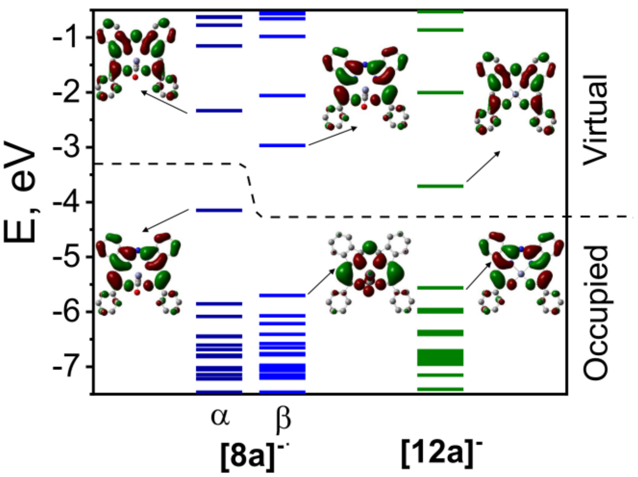

Figure 14. DFT-predicted molecular energy diagram and frontier molecular orbitals of one-electron reduced **[8a]**$^{\cdot-}$ and two-electron reduced **[12a]**$^{-}$ zinc complexes.

The DFT-predicted molecular energy diagram and images of the frontier orbital for the single-electron reduced **[8a]**$^{\cdot-}$ complex (radical-anion form) are shown in Figure 14. As expected, the DFT-predicted SOMO (α,β–156) resembles "half" of the porphyrin a_{1u} orbital, which used to be the LUMO in a starting **8a**, HOMO (α,β–155) resembles "half" of the porphyrin a_{2u} orbital, and the LUMO (α,β–157) resembles the LUMO+1 orbital in the starting **8a**. The TDDFT-predicted UV-Vis spectrum of the radical-anion correlates well with the experimental data (Figure 15). Indeed, the low-energy, "radical-anion" band observed in the NIR region at ~1200 nm is dominated by the SOMO to LUMO (α–156 → α–157) single-electron excitation (predicted at 1084 nm). Similarly, HOMO to SOMO single-electron excitation (β–155 → β–156) provides a major contribution to the second excited state predicted at 631 nm, which correlate well with the experimentally observed band at 637 nm. Higher-energy part of the experimental UV-Vis spectrum of a one-electron reduced [**8a]**$^{\cdot-}$ complex is also well reproduced by the TDDFT calculations.

We also elucidated electronic structures of the two-electron reduced aza-BODIPY like *B*,*O*-chelated systems **11a-c** and zinc complex **[12a]**$^{-}$. In all cases, the HOMO resembles the "half" of the porphyrin a_{1u} orbital, and the LUMO resembles the "half" of the porphyrin a_{2u} orbital,[73,74] which is typical for the BODIPY and aza-BODIPY compounds. It is not surprising to see then that the energy of TDDFT-predicted aza-BODIPY like transition is significantly red-shifted compared to the MB-DIPYs **[5a-c]**$^{-}$, **5a-c**, and **8a-c**. Indeed, TDDFT calculations predict that the *B*,*O*-chelated compounds **11a-c** should have BODIPY-like absorption in the NIR region around 820, 840 and 880 nm, respectively, with an excellent agreement to experimental data (Figure 15). As expected, this transition can be described as almost pure HOMO to LUMO single-electron excitation. In the case of zinc complex **[12a]**$^{-}$, TDDFT calculations clearly underestimate the vertical excitation energies of this complex although provide reasonable qualitative agreement with the experimental spectrum of this compound (Figure 9).

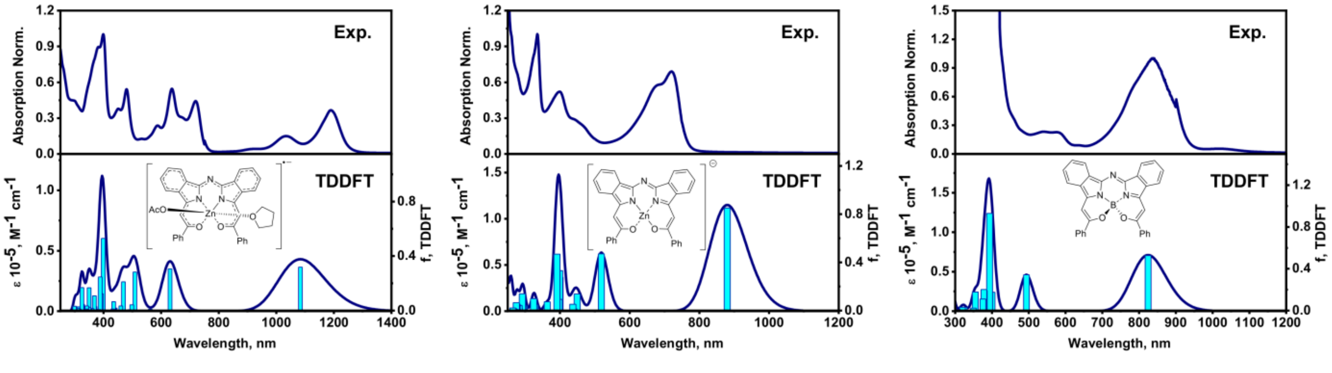

Figure 15. TD DFT-predicted electronic spectra of one-electron reduced **[8a]**$^{\cdot-}$ and two-electron reduced **[12a]**$^{-}$ zinc complexes, as well as two-electron reduced *B*,*O*-chelated aza-BDP **11a.**

In particular, similar to *B,O*-chelated compounds **11a-c**, the lowest energy band correlates well with the first excited state that is almost pure HOMO to LUMO single-electron excitation. The strong band observed at ~420 nm correlate with a second excited state, which, again, similarly to the *B,O*-chelated compounds **11a-c**, is dominated by the HOMO to LUMO+1 single-electron excitation. Finally, three closely energy spaced excited states (excited states 6, 7, and 9) form the strong absorption band observed experimentally at 400 nm. Overall, DFT and TDDFT calculations are suggesting that upon stepwise reduction of the initial DBP compound, their transforms into a classic aza-BODIPY chromophores with intense NIR absorption.

CONCLUSIONS

We report here a new synthetic strategy for preparation of a series of isoindolin-1-imines **3a-c** and isoindolin-1-ones **4a-c** from widely available aromatic ketones and phthalonitrile using several reaction routes. The isoindolin-1-ones **4a-c** can form fluorescent BF$_2$ complexes in solution and solid state. The isoindolin-1-imines **3a-c** undergo self-condensation reaction that leads to the formation of a novel class of *benzo*-fused, highly electron-deficient core-extended azadipyrromethene chromophores (“MB-DIPY”) **[5a-c]**$^-$. The influence of temperature, catalyst, as well as the template ions on the self-condensation reaction rate, yield, and stereoselectivity, was examined in detail. MB-DIPYs **[5a-c]**$^-$ can be hydrolyzed to the metal-free ligands **5a-c** or used for the formation of zinc derivatives **8a-c**. New chromophores (in the form of sodium and zinc complexes as well as metal-free ligands) were characterized by NMR, X-ray, UV-Vis, fluorescence, and high-resolution mass spectroscopies, while their redox properties were probed by electrochemical, spectroelectrochemical, or chemical reduction approaches that reveal their remarkable electron-accepting nature. Stepwise one- and two-electron reduction of the new, core-extended azadipyrromethenes and their zinc complexes was investigated by spectroscopic and spectroelectrochemical methods. Both one- and two-electron reduced forms of all zinc complexes studied have strong absorption in the NIR region up to ~1200 nm. Unstable in solution, NIR absorbing boron derivatives of two-electron reduced ligands **9a-c** (**10a-c** and **11a-c**) were also characterized by mass speacometry and UV-vis spectroscopy. Unusual spectroscopic and electrochemical properties of these dyes were correlated with their electronic structures and excited states nature predicted by the DFT and TDDFT calculations. Despite some structural similarities with well-known aza-BODIPY and azadipyrromethene chromophores, the new systems differ remarkably from them in optical, emission, and redox properties.

EXPERIMENTAL SECTION

Materials. Solvents were purified using standard approaches: THF, 1,4-dioxane, and toluene were dried over sodium metal and benzophenone, DMF and DCM were dried over phosphorous(V) oxide. Phthalonitrile **1**, aromatic ketones **2a-c**, potassium *tert*-butoxide, sodium hydride, LDA, 1.6 M *n*-BuLi, sodium triacetoxyborohydride (STAB), zinc acetate dihydrate, were purchased from Sigma Aldrich. All air-sensitive reactions were carried out under dry argon atmosphere using Schlenk-tube and vacuum-line techniques.

Spectroscopy Measurements. Jasco-V770 spectrophotometer was used to collect UV-Vis data. Steady-state fluorescence studies were performed on Horiba PTI QuantaMaster system. Electrochemical cyclic voltammetry (CV) and differential pulse voltammetry (DPV) measurements were conducted using a CHI-620 C electrochemical analyzer utilizing a three-electrode scheme with platinum working, auxiliary and Ag/AgCl reference electrodes. DCM was used as solvent and 0.1 M solution of tetrabutylammonium perchlorate (TBAP) was used as supporting electrolyte. In all cases, experimental redox potentials were corrected using decamethylferrocene (Fc*H) as an internal standard. NMR spectra were recorded a Bruker Avance instrument with a 300 MHz frequency for protons and 75 MHz frequency for carbons. Chemical shifts are reported in parts per million (ppm) and referenced to the residual proton resonance of the deuterated solvent (CDCl$_3$ = δ 7.26; DMSO-d_6 = δ 2.50), and carbon spectra are referenced to the carbon resonances of the solvent (CDCl$_3$ = δ 77.16; DMSO-d_6 = δ 39.52). High-resolution mass spectra of all new compounds were recorded using a Bruker micrOTOF-QIII. All exact mass measurements showed an error of less than 5 ppm. Melting points were determined by a Stuart SMP10 apparatus and are uncorrected.

General procedure for the synthesis of compounds 3a-c. To the solution of aromatic ketones **2a-c** (20 mmol) in dry DMF (200 mL) solid sodium hydride (40 mmol, 960 mg, 2 eq.) was added portionwise at -20 °C (at 0 °C for **2b**) under argon atmosphere and stirred for 5 min at this temperature. Then, the solution of phthalonitrile **1** (20.4 mmol, 2610 mg, 1.2 eq.) in dry DMF (25 mL) was slowly added. The resulting mixture was stirred at -20 °C for 30 min, then at 0°C for 1 hour, and at room temperature for 6 hours. Then the solution was slowly added into the iced water and neutralized with saturated aqueous ammonium chloride solution. After additional stirring for 1 hour the resulting precipitate was collected by vacuum filtration and air dried.

2-[(1*Z*)-3-imino-2,3-dihydro-1H-isoindol-1-ylidene]-1-phenylethan-1-one (3a). Isolated yield 4.6 g (93 %); Mp: 144 – 145 °C; ^{1}H NMR (300 MHz, CDCl$_3$) δ 10.83 (s, 1H), 8.04 – 8.02 (m, 2H), 7.85 – 7.81 (m, 2H), 7.67 -7.62 (m, 2H), 7.57 - 7.48 (m, 3H), 6.73 (s, 1H); ^{13}C{^{1}H} NMR (75 MHz, CDCl$_3$) δ 191.1, 151.7, 139.1, 136.4, 132.4, 131.6, 128.7, 127.8, 122.2, 121.3, 91.1.; ^{1}H NMR (300 MHz, DMSO-d_6) δ 11.25 (br.s., 1H), 9.06 (br.s., 1H), 8.27 – 8.24 (m, 1H), 8.18 – 8.15 (m, 2H), 7.94 (br.s., 1H), 7.74 – 7.54 (m, 5H), 7.10 (s, 1H); ^{13}C{^{1}H} NMR (75 MHz, DMSO-d_6) δ 189.8, 168.9, 147.6, 137.8, 137.3, 133.3, 133.2, 132.1, 128.8, 128.5, 128.2, 123.4, 122.6, 95.7; HRMS (APCI-TOF) m/z: [M - H]$^-$ Calcd for $C_{16}H_{12}N_2O$ 247.0877; Found 247.0905.

2-[(1*Z*)-3-imino-2,3-dihydro-1H-isoindol-1-ylidene]-1-(4-methoxyphenyl)ethan-1-one (3b). Isolated yield 4.89 g (88 %); Mp: 158 – 160 °C. ^{1}H NMR (300 MHz, CDCl$_3$) δ 8.06 - 8.01 (m, 2H), 7.90 – 7.87 (m, 1H), 7.83 – 7.81 (m, 1H), 7.66 – 7.61 (m, 2H), 7.00 – 6.97 (m, 2H), 6.73 (s, 1H), 3.90 (s, 3H); ^{13}C{^{1}H} NMR (75 MHz, CDCl$_3$) δ 189.8, 163.3, 151.1, 136.6, 132.0, 131.6, 131.5, 130.1, 122.4, 121.3, 114.3, 113.9, 91.1, 55.6; ^{1}H NMR (300 MHz, DMSO-d_6) δ 10.49 (br.s., 2H), 8.32 (d, J_{HH} = 7.4 Hz, 1H), 8.19 (d, J_{HH} = 8.8 Hz, 2H), 8.04 (d, J_{HH} = 7.0 Hz, 1H), 7.79 – 7.69 (m, 2H), 7.25 (s, 1H), 7.10 (d, J_{HH} = 8.8 Hz, 2H), 3.87 (s, 3H); ^{13}C{^{1}H} NMR (75 MHz, CDCl$_3$) δ 188.2, 163.0, 160.8, 149.3, 136.7, 132.2, 131.6, 131.1, 130.4, 130.3, 123.0, 122.5, 114.0, 93.1, 55.6; HRMS (APCI-TOF) m/z: [M - H]$^-$ Calcd for $C_{17}H_{14}N_2O_2$ 277.0983; Found 277.0988.

2-[(1*Z*)-3-imino-2,3-dihydro-1H-isoindol-1-ylidene]-1-(thiophen-2-yl)ethan-1-one (3c). Isolated yield 4.8 g (94 %); Mp: 169 – 171 °C; ^{1}H NMR (300 MHz, $CDCl_3$) δ 7.87 -7.78 (m, 3H), 7.66 – 7.62 (m, 2H), 7.17 (dd, J_{HH} = 4.9 Hz, J_{HH} = 3.8 Hz, 1H), 6.56 (s, 1H); $^{13}C\{^1H\}$ NMR (75 MHz, $CDCl_3$) δ 183.5, 151.4, 146.2, 136.3, 133.0, 131.7, 130.5, 128.3, 122.5, 121.4, 91.5; ^{1}H NMR (300 MHz, DMSO-*d*$_6$) δ 10.92 (br.s., 1H), 9.10 (br.s., 1H), 8.21 – 8.19 (m, 2H), 7.98 – 7.93 (m, 2H), 7.74 – 7.68 (m, 4H), 7.30 (dd, J_{HH} = 4.9 Hz, J_{HH} = 3.8 Hz, 1H), 6.99 (s, 1H); $^{13}C\{^1H\}$ NMR (75 MHz, $CDCl_3$) δ 182.5, 160.0, 150.6, 146.6, 136.6, 134.0, 131.6, 131.5, 131.4, 128.7, 122.4, 122.2, 90.8; HRMS (APCI-TOF) m/z: $[M - H]^-$ Calcd for $C_{14}H_{10}N_2OS$ 253.0441; Found 253.0414.

General procedure for the synthesis of compounds 4a-c
To the solution of isoindol-1-imines **3a-c** (4 mmol) in ethanol (40 mL), concentrated hydrochloric acid (2 mL) was added. The resulting mixture was refluxed for 8 hours. After cooling to room temperature, the solution was diluted with water (40 mL) and stirred for another 30 min. Then, the resulting precipitate was collected by filtration and air dried to give pure isoindolin-1-ones **4a-c**.

(3*Z*)-3-(2-oxo-2-phenylethylidene)-2,3-dihydro-1H-isoindol-1-one(4a). Isolated yield 747 mg (75 %); Mp: 164 – 166 °C; ^{1}H NMR (300 MHz, $CDCl_3$) δ 10.61 (s, 1H), 8.06 – 8.03 (m, 2H), 7.93 – 7.90 (m, 1H), 7.85 – 7.83 (m, 1H), 7.72 – 7.50 (m, 5H), 6.89 (s, 1H); $^{13}C\{^1H\}$ NMR (75 MHz, $CDCl_3$) δ 191.2, 169.2, 148.6, 138.6, 137.3, 133.1, 133.0, 132.1, 129.5, 128.9, 128.1, 124.4, 121.3, 94.9; HRMS (APCI-TOF) m/z: $[M - H]^-$ Calcd for $C_{16}H_{11}NO_2$ 248.0717; Found 248.0688.

(3*Z*)-3-[2-(4-methoxyphenyl)-2-oxoethylidene]-2,3-dihydro-1H-isoindol-1-one (4b). Isolated yield 860 mg (77 %); Mp: 182 – 184 °C; ^{1}H NMR (300 MHz, $CDCl_3$) δ 10.64 (s, 1H), 8.07 – 8.02 (m, 2H), 7.92 – 7.89 (m, 1H), 7.85 – 7.82 (m, 1H), 7.71 – 7.61 (m, 2H), 7.02 – 6.98 (m, 2H), 6.86 (s, 1H), 3.90 (s, 3H); $^{13}C\{^1H\}$ NMR (75 MHz, $CDCl_3$) δ 189.7, 169.2, 163.7, 147.9, 137.4, 132.9, 131.9, 131.5, 130.5, 129.5, 124.4, 121.1, 114.1, 94.9, 55.7; HRMS (APCI-TOF) m/z: $[M - H]^-$ Calcd for $C_{17}H_{13}NO_3$ 278.0823; Found 278.0847.

(3*Z*)-3-[2-oxo-2-(thiophen-2-yl)ethylidene]-2,3-dihydro-1H-isoindol-1-one (4c). Isolated yield 867 mg (85 %); Mp: 220 – 222 °C; ^{1}H NMR (300 MHz, $CDCl_3$) δ 10.47 (s, 1H), 7.92 – 7.89 (m, 1H), 7.86 -7.82 (m, 2H), 7.72 – 7.62 (m, 3H) 7.21 (dd, J_1 = 4.9 Hz, J_2 = 3.8 Hz, 1H), 6.70 (s, 1H); $^{13}C\{^1H\}$ NMR (75 MHz, $CDCl_3$) δ 183.4, 168.9, 148.2, 145.8, 137.0, 134.1, 133.0, 132.1, 131.4, 129.5, 128.5, 124.4, 121.3, 95.3; HRMS (APCI-TOF) m/z: $[M - H]^-$ Calcd for $C_{14}H_9NO_2S$ 254.0281; Found 254.0257.

General procedure for the synthesis of dyes $[5a\text{-}c]^-$:
To the solution of isoindol-1-imines **3a-c** (4 mmol) in dry 1,4-dioxane (100 mL), sodium hydride dust (2.4 mmol, 58 mg, 0.6 eq.) was added under argon atmosphere. The solution was stirred for 5 min at room temperature, then under reflux conditions for 2h. After cooling to room temperature the resulting intense purple solution was diluted with dry hexane (100 mL) and left for 3 hours for the crystallization. After 3 h, the resulting black product was filtered off, washed with dry hexane, and dried under high vacuum.

Compound $[5a]^-$. Isolated yield 772 mg (77 %); Mp: >300 °C; ^{1}H NMR (300 MHz, $(CD_3)_2CO$-*d*$_6$) δ 8.31 – 8.29 (m, 4H), 8.15 – 8.12 (m, 2H), 8.07 – 8.04 (m, 2H), 7.69 – 7.53 (m, 10H), 7.41 (s, 2H); $^{13}C\{^1H\}$ NMR (75 MHz, $(CD_3)_2CO$-*d*$_6$) δ 191.5, 165.3, 143.2, 141.8, 141.4, 133.2, 130.8, 130.4, 129.5, 129.1, 122.9, 121.4, 102.7; HRMS (APCI-TOF) m/z: $[M - H]^-$ Calcd for $C_{32}H_{20}N_3O_2$ 478.1561; Found 478.1550.

Compound $[5b]^-$. Isolated yield 561 mg (50 %); Mp: >300 °C;^{1}H NMR (300 MHz, $(CD_3)_2CO$-*d*$_6$) δ 8.33 (d, J_{HH} = 8.9 Hz, 4H), 8.11 – 8.10 (m, 2H), 8.04 – 8.03 (m, 2H), 7.59 – 7.50 (m, 4H), 7.39 (s, 2H), 7.13 (d, J_{HH} = 8.9 Hz, 4H), 3.94 (s, 6H); $^{13}C\{^1H\}$ NMR (75 MHz, $(CD_3)_2CO$-*d*$_6$) δ 190.0, 164.6, 164.3, 143.4, 141.9, 134.2, 131.4, 130.5, 130.2, 122.8, 121.3, 114.6, 102.7, 55.9; HRMS (APCI-TOF) m/z: $[M - H]^-$ Calcd for $C_{34}H_{24}N_3O_4$ 538.1772; Found 538.1761.

Compound $[5c]^-$. Isolated yield 822 mg (81 %); Mp: >300 °C;^{1}H NMR (300 MHz, $(CD_3)_2CO$-*d*$_6$) δ 8.27 (dd, J_{HH} = 3.8 Hz, J_{HH} = 1.1 Hz, 2H), 8.11 – 8.09 (m, 2H), 8.06 – 8.03 (m, 2H), 7.93 (dd, J_{HH} = 5.0 Hz, J_{HH} = 1.1 Hz, 2H), 7.60 – 7.51 (m, 4H), 7.32 – 7.29 (m, 4H); $^{13}C\{^1H\}$ NMR (75 MHz, $(CD_3)_2CO$-*d*$_6$) δ 184.0, 176.6, 165.0, 149.5, 143.06, 141.9, 134.8, 132.4, 130.8, 130.4, 129.4, 129.2, 123.0, 121.4, 102.7; HRMS (APCI-TOF) m/z: $[M - H]^-$ Calcd for $C_{28}H_{16}N_3O_2S_2$ 490.0689; Found 490.0676.

General procedure for the synthesis of compounds 5a-c
The suspension of anionic dye $[5a\text{-}c]^-$ (0.5 mmol) in dry ethanol (8 mL) was treated with glacial acetic acid (1 mmol, 60 mg, 2 eq.) and stirred for 1 hour at room temperature. The resulting brown precipitate was collected by filtration and vacuum dried.

Compound 5a. Isolated yield 139 mg (58 %); Mp: 200 – 202 °C; ^{1}H NMR (300 MHz, $(CDCl_3)$ δ 13.38 (s, 1H), 8.15 – 8.12 (m, 4H), 8.09 – 8.06 (m, 2H), 7.88 – 7.85 (m, 2H), 7.61 – 7.58 (m, 4H), 7.52 – 7.43 (m, 6H), 7.07 (s, 2H); $^{13}C\{^1H\}$ NMR (75 MHz, $(CDCl_3)$ δ 190.8, 167.6, 151.9, 138.7, 136.3, 133.1, 132.9, 132.7, 132.3, 130.9, 130.6, 129.2, 128.9, 128.9, 128.8, 128.4, 128.2, 123.0, 121.5, 121.5, 120.9, 106.8, 97.0; HRMS (APCI positive) Calcd for $C_{32}H_{21}N_3O_2$ $[M + H]^+$: 480.1707, Found 480.1702.

Compound 5b. Isolated yield 172 mg (64 %); Mp: 164 – 166 °C; ^{1}H NMR (300 MHz, $CDCl_3$) δ 13.34 (s, 1H), 8.13 – 8.10 (m, 4H), 8.08 – 8.05 (m, 2H), 7.84 -7.84 (m, 2H), 7.59 – 7.57 (m, 4H), 7.01 (s, 2H), 6.94 – 6.91 (m, 4H), 3.82 (s, 6H); $^{13}C\{^1H\}$ NMR (75 MHz, $CDCl_3$) δ 189.5, 167.3, 163.4, 151.2, 138.8, 136.3, 131.9, 131.6, 130.8, 130.4, 122.9, 120.8, 113.6, 107.1, 55.6; HRMS (APCI positive) Calcd for $C_{34}H_{25}N_3O_4$ $[M + H]^+$: 540.1918, Found 540.1916.

Compound 5c. Isolated yield 135 mg (55 %); Mp: 174 – 176 °C; ^{1}H NMR (300 MHz, $CDCl_3$) δ 13.25 (s, 1H), 8.08 – 8.06 (m, 2H), 7.90 (dd, J_{HH} = 3.8 Hz, J_{HH} = 1.0 Hz, 2H), 7.86 – 7.82 (m, 2H), 7.65 (dd, J_{HH} = 4.9 Hz, J_{HH} = 1.0 Hz, 2H), 7.60 – 7.56 (m, 4H), 7.13 (dd, J_{HH} = 4.9 Hz, J_{HH} = 3.8 Hz, 2H), 6.93 (s, 2H); $^{13}C\{^1H\}$ NMR (75 MHz, $CDCl_3$) δ 182.8, 167.6, 151.7, 146.3, 138.7, 1363, 133.8, 132.6, 131.0, 130.6, 128.0, 123.0, 120.9, 106.7; HRMS (APCI positive) Calcd for $C_{28}H_{17}N_3O_2S_2$ $[M + H]^+$:492.0835, Found 492.0838.

General procedure for the synthesis compounds 7a-c.
To the solution of isoindolin-1-ones **4a-c** (0.4 mmol) in dry DCM (10 mL), *N,N*-diisopropylethylamine (DIPEA) (1.2 mmol, 155 mg, 3 eq.), and boron trifluoride diethyl etherate (2.4 mmol, 341 mg, 6 eq.) were added. The resulting mixture was stirred for 1 hour. Then the solution was quenched with water, the organic layer was washed with water (2 ^{x} 50 mL), saturated brine solution (20 mL), dried over Na_2SO_4, and evaporated to dryness. The crude product was stirred in ethanol (20 ml) for 30 min. Then the resulting precipitate was collected by vacuum filtration and air dried.

1,1-difluoro-3-phenyl-9H-[1,3,2]oxazaborinino[4,3-a]isoindol-9-one (7a). Isolated yield 89 mg (75 %); Mp: 260 – 262 °C; ^{1}H NMR (300 MHz, $CDCl_3$) δ 8.24 – 8.22 (m, 2H), 8.00 – 7.97 (m, 1H), 7.91 – 7.88 (m, 1H), 7.82 – 773 (m, 3H), 7.63 – 7.57 (m, 2H), 6.97 (s, 1H); HRMS (APCI-TOF) m/z: $[M - H]^-$ Calcd for $C_{16}H_{10}NO_2BF_2$ 297.0781; Found 297.0769.

1,1-difluoro-3-(4-methoxyphenyl)-9H-[1,3,2]oxazaborinino[4,3-a]isoindol-9-one (7b). Isolated yield 93 mg (71 %); Mp: 285 – 287 °C; ^{1}H NMR (300 MHz, $CDCl_3$) δ 8.25 (d, *J* = 9.1 Hz, 2H), 7.98 -7.95 (m, 1H), 7.88 – 7.85 (m, 1H), 7.78 – 7.73 (m, 2H), 7.07 (d, *J* = 9.1 Hz, 2H), 6.89 (s, 1H), 3.96 (s, 2H); HRMS (APCI-TOF) m/z: $[M - H]^-$ Calcd for $C_{17}H_{12}NO_3BF_2$ 327.0887; Found 327.0883.

1,1-difluoro-3-(thiophen-2-yl)-9H-[1,3,2]oxazaborinino[4,3-a]isoindol-9-one (7c). Isolated yield 90 mg (74 %); Mp: 287 – 289 °C; ^{1}H NMR (300 MHz, $CDCl_3$) δ 8.20 (dd, J_1 = 4.0 Hz, J_2 = 1.1 Hz, 1H), 8.01 – 7.98 (m, 2H), 7.88 – 7.85 (m, 1H), 7.81 – 7.72 (m, 2H), 7.35 (dd, J_1 = 4.8 Hz, J_2 = 4.0 Hz, 1H), 6.76 (s, 1H); HRMS (APCI-TOF) m/z: $[M - H]^-$ Calcd for $C_{14}H_8NO_2SBF_2$ 303.0345; Found 303.0346.

General procedure for the synthesis of compounds 8a-c
To the solution of dye **[5a-c]**$^-$ (0.1 mmol) in dry THF (10 mL) zinc acetate dihydrate (0.11 mmol, 24 mg, 1.1 eq.) was added. The resulting mixture was stirred for 1 hour at room temperature. Then the resulting precipitate was collected by filtration, washed with hexane and vacuum dried.

Compound 8a. Isolated yield 56 mg (83 %); Mp: 235 – 237 °C; ^{1}H NMR (300 MHz, $CDCl_3$) δ 8.34 - 8.31 (m, 4H), 8.18 – 8.15 (m, 2H), 7.92 – 7.89 (m, 2H), 7.67 – 7.56 (m, 10H), 7.35 (s, 2H), 3.77 – 3.73 (m, 2H), 1.92 – 1.87 (m, 2H, THF) 1.79 (s, 3H); HRMS (APCI-TOF) m/z: $[M + H]^+$ Calcd for $C_{32}H_{20}N_3O_2Zn$ 542.0841; Found 542.0853.

Compound 8b. Isolated yield 51 mg (70 %); Mp: 242 – 244 °C; ^{1}H NMR (300 MHz, $CDCl_3$) δ 8.35 (d, *J* = 8.9 Hz, 4H), 8.16 – 8.12 (m, 2H), 7.93 7.88 (m, 2H), 7.63 – 7.58 (m, 4H), 7.32 (s, 2H), 7.07 (d, *J* = 8.9 Hz, 4H), 3.95 (s, 6H), 3.77 – 3.72 (m, 3H), 1.88 – 1.85 (m, 5H); HRMS (APCI-TOF) m/z: $[M + H]^+$ Calcd for $C_{34}H_{24}N_3O_4Zn$ 602.1053; Found 602.1053.

Compound 8c. Isolated yield 55 mg (80 %); Mp: 251 – 253 °C; ^{1}H NMR (300 MHz, $CDCl_3$) δ 8.16 – 8.11 (m, 5H), 7.89 – 7.87 (m, 2H), 7.82 – 7.80 (m, 2H), 7.64 – 7.56 (m, 5H), 7.14 (s, 2H), 3.77 – 3.72 (m, 3H, THF), 1.88 – 1.86 (m, 7H); HRMS (APCI-TOF) m/z: $[M + H]^+$ Calcd for $C_{28}H_{16}N_3O_2S_2Zn$ 553.9970; Found 553.9975.

General procedure for the synthesis of compounds 11a-c
The mixture of dyes **5a-c** (0.1 mmol) and sodium triacetoxyborohydride (STAB) (0.25 mmol, 53 mg, 2.5 eq.) was refluxed in dry toluene for 1-2 min until intense brown to green solution of *B,O*-chelated dyes **11a-c** formed. Due to the low stability of the obtained dyes they were immediately subjected to HRMS and UV-Vis spectroscopy analyses.

Compound 11a. Reaction time – 1 min. UV/Vis (Toluene): λ_{max}=840 nm; HRMS (APCI-TOF) m/z: $[M + H]^+$ Calcd for $C_{32}H_{20}N_3O_2B$ 489.1660; Found 489.1645.

Compound 11b. Reaction time – 2 min. UV/Vis (Toluene): λ_{max}=870 nm; HRMS (APCI-TOF) m/z: $[M - H]^-$ Calcd for $C_{34}H_{24}N_3O_4B$ 550.1939; Found 550.1920.

Compound 11c. Reaction time – 2 min. UV/Vis (Toluene): λ_{max}=910 nm; HRMS (APCI-TOF) m/z: $[M + H]^+$ Calcd for $C_{28}H_{16}N_3O_2S_2B$ 501.0788; Found 501.0788.

General procedure for the synthesis of one- and two-electron reduced compounds [8a-c]$^{\cdot-}$ **and [12a-c]**$^-$**.** The suspension of appropriate zinc(II) compexes **8a-c** (0.1 mmol) in dry THF (10 mL) was treated with sodium borohydride (0.25 mmol, 10 mg, 2.5 eq.) under argon atmosphere. The resulting mixture was stirred for 10 min yielding **[8a-c]**$^{\cdot-}$ as a deep green solution. Then the solution was treated with 25% methanolic tetramethylammonium hydroxide solution (0.1 mmol, 37 mg, 1 eq.) and stirred for another 5 min yielding green solution of two-electron reduced anionic zinc(II) complexes **[12a-c]**$^-$. Due to the low stability of the obtained dyes they were immediately subjected to UV-Vis absorption and fluorescence (in the case of dyes **[12a-c]**$^-$) spectroscopy analyses.

Compound [8a]$^{\cdot-}$. UV/Vis (THF): λ_{max}=1190, 1030, 720, 637, 480, 400 nm.

Compound [8b]$^{\cdot-}$. UV/Vis (THF): λ_{max}=1185, 1030, 718, 642, 480, 402 nm.

Compound [8c]$^{\cdot-}$. UV/Vis (THF): λ_{max}=1236, 1070, 740, 645, 490, 408 nm.

Compound [12a]$^-$. UV/Vis (THF): λ_{max}= 720, 680, 400, 335 nm; fluorescence (THF): λ_{ex}=710 nm; λ_{em}=753 nm.

Compound [12b]$^-$. UV/Vis (THF): λ_{max}= 712, 665, 440, 390, 336 nm; fluorescence (THF): λ_{ex}=710 nm; λ_{em}=750 nm.

Compound [12c]$^-$. UV/Vis (THF): λ_{max}= 730, 692, 446, 403, 335 nm; fluorescence (THF): λ_{ex}=710 nm; λ_{em}=763 nm.

X-ray data collection, solution and refinement for 3b.

A light yellow, multi-faceted rod of suitable size (0.200 x 0.070 x 0.040 mm) was selected from a representative sample of crystals of the same habit using an optical microscope and mounted onto a MiTiGen loop. X-ray data were obtained on a Bruker D8 QUEST ECO CMOS diffractometer (Mo sealed X-ray tube, K_α = 0.71073 Å) at 150 K. All diffractometer manipulations, including data collection, integration and scaling were carried out using the Bruker APEX3 software suite.[75] Despite collecting a number of datasets of which this represents the best, less than ideal quality data was ultimately obtained, resulting in a number of alerts highlighted by vrf reports. We are nevertheless confident in atom assignment and connectivity. An absorption correction was applied using SADABS.[76] The space group was determined on the basis of systematic absences and intensity statistics and the structure was solved by direct methods and refined by full-matrix least squares on F^2. The structure was solved in the monoclinic space group $P2_1$/c using XS[2] (incorporated in SHELXTL). No obvious missed symmetry was reported by PLATON.[77] All non-hydrogen atoms were refined with anisotropic thermal parameters. Hydrogen atoms were placed in idealized positions and refined using a riding model. The structure was refined (weighted least squares refinement on F^2) and the final least-squares refinement converged to R_1 = 0.0995 ($I > 2\sigma(I)$, 1078 data) and wR_2 = 0.2576 (F^2, 2736 data, 228 parameters).

X-ray data collection, solution and refinement for 3c

A dark purple, multi-faceted block of suitable size (0.143 x 0.092 x 0.091 mm) and quality was selected from a representative sample of crystals of the same habit using an optical microscope and mounted onto a MiTiGen loop. X-ray data were obtained on a Bruker D8 QUEST ECO CMOS diffractometer (Mo sealed X-ray tube, K_α = 0.71073 Å) at 150 K. All diffractometer manipulations, including data collection, integration and scaling were carried out using the Bruker APEX3 software suite.[75] An absorption correction was applied using SADABS.[76] The space group was determined on the basis of systematic absences and intensity statistics and the structure was solved by direct methods and refined by full-matrix least squares on F^2. The structure was solved in the monoclinic space group $P2_1$/c using XS[2] (incorporated in SHELXTL). No obvious missed symmetry was reported by PLATON.[77] “Flip”-type disorder[4] was observed for two thiophenyl side chains, wherein different types of atoms (sulfur and carbon) occupy positions that are close to each other. This influences their thermal parameters, which were therefore equated for each pair of disordered atoms in the disordered rings. All non-hydrogen atoms were refined with anisotropic thermal parameters. Hydrogen atoms were placed in idealized positions and refined using a riding model, with the exception of those of a co-crystallized molecule of water and an N-*H* engaged in hydrogen bonding, which were located from the difference map. The structure was refined (weighted least squares refinement on F^2) and the final least-squares refinement converged to R_1 = 0.0442 ($I > 2\sigma(I)$, 2348 data) and wR_2 = 0.1097 (F^2, 2883 data, 185s parameters).

X-ray data collection, solution and refinement for 4c

A light brown, multi-faceted block of suitable size (0.298 x 0.244 x 0.125 mm) and quality was selected from a representative sample of crystals of the same habit using an optical microscope and mounted onto a MiTiGen loop. X-ray data were obtained on a Bruker D8 QUEST ECO CMOS diffractometer (Mo sealed X-ray tube, K_α = 0.71073 Å) at 150 K. All diffractometer manipulations, including data collection, integration and scaling were carried out using the Bruker APEX3 software suite.[75] An absorption correction was applied using SADABS.[76] The space group was determined on the basis of systematic absences and intensity statistics and the structure was solved by direct methods and refined by full-matrix least squares on F^2. The structure was solved in the monoclinic space group $C2$/c using XS[2] (incorporated in SHELXTL). No obvious missed symmetry was reported by PLATON.[77] All non-hydrogen atoms were refined with anisotropic thermal parameters. Hydrogen atoms were placed in idealized positions and refined using a riding model. The structure was refined (weighted least squares refinement on F^2) and the final least-squares refinement converged to R_1 = 0.0382 ($I > 2\sigma(I)$, 3071 data) and wR_2 = 0.1082 (F^2, 3456 data, 163 parameters).

X-ray data collection, solution and refinement for 5b

An orange, multi-faceted plate of suitable size (0.176 x 0.149 x 0.033 mm) and quality was selected from a representative sample of crystals of the same habit using an optical microscope and mounted onto a MiTiGen loop. X-ray data were obtained on a Bruker D8 QUEST ECO CMOS diffractometer (Mo sealed X-ray tube, K_α = 0.71073 Å) at 296 K. All diffractometer manipulations, including data collection, integration and scaling were carried out using the Bruker APEX3 software suite.[75] An absorption correction was applied using SADABS.[76] The space group was determined on the basis of systematic absences and intensity statistics and the structure was solved by direct methods and refined by full-matrix least squares on F^2. The structure was solved in the monoclinic space group $P2_1$/c using XS[2] (incorporated in SHELXTL). No obvious missed symmetry was reported by PLATON.[77] All non-hydrogen atoms were refined with anisotropic thermal parameters. Hydrogen atoms were placed in idealized positions and refined using a riding model. The structure was refined (weighted least squares refinement on F^2) and the final least-squares refinement converged to R_1 = 0.0679 ($I > 2\sigma(I)$, 2297 data) and wR_2 = 0.1452 (F^2, 4473 data, 372 parameters).

X-ray data collection, solution and refinement for $[5c]^-$

A dark purple, multi-faceted block of suitable size (0.280 x 0.254 x 0.198 mm) and quality was selected from a representative sample of crystals of the same habit using an optical microscope and mounted onto a MiTiGen loop. X-ray data (R_{int} = 0.0354) were obtained on a Bruker D8 QUEST ECO CMOS diffractometer (Mo sealed X-ray tube, K_α = 0.71073 Å) at 150 K. All diffractometer manipulations, including data collection, integration and scaling were carried out using the Bruker APEX3 software suite.[75] An absorption correction was applied using SADABS.[76] The space group was determined on the basis of systematic absences and intensity statistics and the structure was solved by direct methods and refined by full-matrix least squares on F^2. The structure was solved in the monoclinic space group $P2_1$/c using XS[2] (incorporated in SHELXTL). No obvious missed symmetry was reported by PLATON.[77] Non-merohedral twinning about a 2-axis was detected using TWINROTMAT embedded within PLATON[77] and the appropriate twin law applied. “Flip”-type disorder[4] was observed for two of four thiophenyl side chains, wherein different types of atoms (sulfur and carbon) occupy positions that are close to each other. This influences their thermal parameters, which were therefore equated for each pair of disordered atoms in the disordered rings. All non-hydrogen atoms were refined with anisotropic thermal parameters. Hydrogen atoms were placed in idealized positions and refined using a riding model. The structure was refined (weighted least squares refinement on F^2) and the final least-squares refinement converged to R_1 = 0.0451 ($I >$

$2\sigma(I)$, 15571 data) and $wR_2 = 0.1210$ (F^2, 18245 data, 652 parameters).

X-ray data collection, solution and refinement for 7b

A dark, multi-faceted block of suitable size (0.100 x 0.080 x 0.050 mm) and quality was selected from a representative sample of crystals of the same habit using an optical microscope and mounted onto a MiTiGen loop. X-ray data were obtained on a Bruker D8 QUEST ECO CMOS diffractometer (Mo sealed X-ray tube, $K_\alpha = 0.71073$ Å) at 150 K. All diffractometer manipulations, including data collection, integration and scaling were carried out using the Bruker APEX3 software suite.[75] An absorption correction was applied using SADABS.[76] The space group was determined on the basis of systematic absences and intensity statistics and the structure was solved by direct methods and refined by full-matrix least squares on F^2. The structure was solved in the triclinic space group P-1 using XS[2] (incorporated in SHELXTL). No obvious missed symmetry was reported by PLATON.[77] All non-hydrogen atoms were refined with anisotropic thermal parameters. Hydrogen atoms were placed in idealized positions and refined using a riding model. Non-merohedral twinning was detected using TWINROTMAT embedded within PLATON[77] and the appropriate twin law applied. The structure was refined (weighted least squares refinement on F^2) and the final least-squares refinement converged to $R_1 = 0.1067$ ($I > 2\sigma(I)$, 2732 data) and $wR_2 = 0.2420$ (F^2, 4921 data, 436 parameters).

X-ray data collection, solution and refinement for 8c

A dark purple, multi-faceted block of suitable size (0.128 x 0.117 x 0.084 mm) and quality was selected from a representative sample of crystals of the same habit using an optical microscope and mounted onto a MiTiGen loop. X-ray data ($R_{int} = 0.0572$) were obtained on a Bruker D8 QUEST ECO CMOS diffractometer (Mo sealed X-ray tube, $K\alpha = 0.71073$ Å) at 150 K. All diffractometer manipulations, including data collection, integration and scaling were carried out using the Bruker APEX3 software suite.[75] An absorption correction was applied using SADABS.[76] The space group was determined on the basis of systematic absences and intensity statistics and the structure was solved by direct methods and refined by full-matrix least squares on F^2. The structure was solved in the monoclinic space group $P2_1$/c using XS[2] (incorporated in SHELXTL). No obvious missed symmetry was reported by PLATON.[77] "Flip"-type disorder[78,79] was observed for one of two thiophenyl side chains, wherein different types of atoms (sulfur and carbon) occupy positions that are close to each other. This influences their thermal parameters, which were therefore equated for each pair of disordered atoms in the disordered rings. All non-hydrogen atoms were refined with anisotropic thermal parameters. Hydrogen atoms were placed in idealized positions and refined using a riding model. A disordered acetic acid solvent molecule was found in the lattice, however the acidic O-H hydrogen could not be satisfactorily modeled for one of two components of the disorder. The structure was refined (weighted least squares refinement on F^2) and the final least-squares refinement converged to $R_1 = 0.0589$ ($I > 2\sigma(I)$, 6879 data) and $wR_2 = 0.1524$ (F^2, 7984 data, 458 parameters).

Combined crystallographic information file containing all X-ray data. CCDC 1935790-1935796 containing the supplementary crystallographic data for this paper. The data can be obtained free of charge from The Cambridge Crystallographic Data Centre via www.ccdc.cam.ac.uk/structures. Mercury[80] was used in all crystallographic images.

ASSOCIATED CONTENT

Supporting Information. The Supporting Information is available free of charge on the ACS Publications website

NMR spectra, HRMS spectra, absorption and emission spectra, electrochemical studies, X-ray crystallography data and CIF files for all new compounds as well as computational details.

Corresponding Author

* Yurii.Zatsikha@umanitoba.ca

* Victor.Nemykin@umanitoba.ca

ORCID

Victor Nemykin: 0000-0003-4345-0848

Yuriy Zatsikha: 0000-0002-9770-7007

David E. Herbert: 0000-0001-8190-2468

Notes

The authors declare no competing financial interests.

ACKNOWLEDGMENT

Generous support from the Minnesota Supercomputing Institute, NSERC, CFI, University of Manitoba, and WestGrid Canada to VN is greatly appreciated.

REFERENCES

(1) Lu, H.; Kobayashi, N. Optically active porphyrin and phthalocyanine systems. *Chem. Rev*. **2016** *116* (10), 6184-6261.
(2) De La Torre, G.; Vazquez, P.; Agullo-Lopez, F.; Torres, T. Role of structural factors in the nonlinear optical properties of phthalocyanines and related compounds. *Chem. Rev*. **2004**, *104* (9), 3723-3750.
(3) Urbani, M.; de la Torre, G.; Nazeeruddin, M. K.; Torres, T. Phthalocyanines and porphyrinoid analogues as hole- and electron-transporting materials for perovskite solar cells. *Chem. Soc. Rev*. **2019**, *48*, 2738-2766.
(4) Urbani, M.; Ragoussi, M.-E.; Nazeeruddin, M. K.; Torres, T. Phthalocyanines for dye-sensitized solar cells. *Coord. Chem. Rev*. **2019**, *381*, 1-64.
(5) Dumoulin, F.; Durmus, M.; Ahsen, V.; Nyokong, T. Synthetic pathways to water-soluble phthalocyanines and close analogs. *Coord. Chem. Rev*. **2010**, *254*, 2792-2847.
(6) Zagal, J. H.; Griveau, S.; Silva, J. F.; Nyokong, T.; Bedioui, F. Metallophthalocyanine-based molecular materials as catalysts for electrochemical reactions. *Coord. Chem. Rev*. **2010**, *254*, 2755-2791.
(7) Pushkarev, V. E.; Tomilova, L. G.; Nemykin, V. N. Historic overview and new developments in synthetic methods for preparation of the rare-earth tetrapyrrolic complexes. *Coord. Chem. Rev*. **2016**, *319*, 110-179.
(8) Vecchi, A.; Galloni, P.; Floris, B.; Dudkin, S. V.; Nemykin, V. N. Metallocenes meet porphyrinoids: Consequences of a "fusion". *Coord. Chem. Rev*. **2015**, *291*, 95-171.
(9) Nemykin, V. N.; Blesener, T. S.; Ziegler, C. J. Photophysics, redox processes, and electronic structures of ferrocenyl-containing BODIPYs, aza-BODIPYs, BOPHYs, transition-metal dipyrromethenes and aza-dipyrromethenes. *Makrogeterotsikly* **2017**, *10*, 9-26.
(10) Lu, H.; Mack, J.; Yang, Y.; Shen, Z. Structural modification strategies for the rational design of red/NIR region BODIPYs. *Chem. Soc. Rev*. **2014**, *43*, 4778-4823.
(11) Ulrich, G.; Ziessel, R.; Harriman, A. The chemistry of fluorescent Bodipy dyes: versatility unsurpassed. *Angew. Chem., Int. Ed.* **2008**, *47*, 1184-1201.

(12) Ziessel, R.; Ulrich, G.; Harriman, A. The chemistry of Bodipy: A new El Dorado for fluorescence tools. *New J. Chem.* **2007**, *31*, 496-501.

(13) Vecchi, A.; Galloni, P.; Floris, B.; Nemykin, V. N. New developments in chemistry of organometallic porphyrins and their analogs. *J. Porphyrins Phthalocyanines* **2013**, *17*, 165-196.

(14) Maligaspe, E.; Pundsack, T. J.; Albert, L. M.; Zatsikha, Y. V.; Solntsev, P. V.; Blank, D. A.; Nemykin, V. N. Synthesis and Charge-Transfer Dynamics in a Ferrocene-Containing Organoboryl aza-BODIPY Donor-Acceptor Triad with Boron as the Hub. *Inorg. Chem.* **2015**, *54*, 4167-4174.

(15) Bessette, A.; Hanan, G. S. Design, synthesis and photophysical studies of dipyrromethene-based materials: insights into their applications in organic photovoltaic devices. *Chem. Soc. Rev.* **2014**, *43*, 3342-3405.

(16) Piyanuch, P.; Sirirak, J.; Kamkaew, A.; Weeranantanapan, O.; Promarak, V.; Burgess, K.; Wanichacheva, N. A Near-Infrared Fluorescence Chemosensor Based on Isothiocyanate-Aza-Bodipy for Cyanide Detection at the Parts per Billion Level: Applications in Buffer Media and Living Cell Imaging. *ChemPlusChem* **2019**, *84*, 252-259.

(17) Kubheka, G.; Achadu, O.; Mack, J.; Nyokong, T. Optical limiting properties of 3,5-diphenyldibenzo-azaBODIPY at 532 nm. *New J. Chem.* **2017**, *41*, 12319-12325.

(18) Strobl, M.; Walcher, A.; Mayr, T.; Klimant, I.; Borisov, S. M. Trace Ammonia Sensors Based on Fluorescent Near-Infrared-Emitting aza-BODIPY Dyes. *Analyt. Chem.* **2017**, *89*, 2859-2865.

(19) Tamgho, I.-S.; Hasheminasab, A.; Engle, J. T.; Nemykin, V. N.; Ziegler, C. J. A New Highly Fluorescent and Symmetric Pyrrole-BF_2 Chromophore: BOPHY. *J. Am. Chem. Soc.* **2014**, *136*, 5623-5626.

(20) Rhoda, H. M.; Chanawanno, K.; King, A. J.; Zatsikha, Y. V.; Ziegler, C. J.; Nemykin, V. N. Unusually Strong Long-Distance Metal-Metal Coupling in Bis(ferrocene)-Containing BOPHY: An Introduction to Organometallic BOPHYs. *Chem. Eur. J.* **2015**, *21*, 18043-18046.

(21) Zatsikha, Y. V.; Nemez, D. B.; Davis, R. L.; Singh, S.; Herbert, D. E.; King, A. J.; Ziegler, C. J.; Nemykin, V. N. Testing the Limits of the BOPHY Platform: Preparation, Characterization, and Theoretical Modeling of BOPHYs and Organometallic BOPHYs with Electron-Withdrawing Groups at β-Pyrrolic and Bridging Positions. *Chem. Eur. J.* **2017**, *23*, 14786-14796.

(22) Boodts, S.; Fron, E.; Hofkens, J.; Dehaen, W. The BOPHY fluorophore with double boron chelation: Synthesis and spectroscopy. *Coord. Chem. Rev.* **2018**, *371*, 1-10.

(23) Sirbu, D.; Woodford, O. J.; Benniston, A. C.; Harriman, A. Photocatalysis and self-catalyzed photobleaching with covalently-linked chromophore-quencher conjugates built around BOPHY. *Photochem. Photobiol. Sci.* **2018**, *17*, 750-762.

(24) Nemykin, V. N.; Lukyanets, E. A. in Handbook of Porphyrin Science, Kadish, K. M.; Smith, K. M.; Guilard, R. (Eds.), World Scientific, Singapore, **2010**, *3*, 1-323.

(25) Donyagina, V. F.; Shimizu, S.; Kobayashi, N.; Lukyanets, E. A. Synthesis of *N,N*-difluoroboryl complexes of 3,3'-diarylazadiisoindolylmethenes. *Tetr. Lett.* **2008**, *49*, 6152-6154.

(26) Claessens, C. G.; Gonzalez-Rodriguez, D.; Rodriguez-Morgade, M. S.; Medina, A.; Torres, T. Subphthalocyanines, Subporphyrazines, and Subporphyrins: Singular Nonplanar Aromatic Systems. *Chem. Rev.* **2014**, *114*, 2192-2277.

(27) Crandall, L. A.; Rhoda, H. M.; Nemykin, V. N.; Ziegler, C. J. Boron templated synthesis of a BODIPY analogue from a phthalocyanine precursor. *New J. Chem.* **2016**, *40*, 5675-5678.

(28) Elvidge, J. A.; Linstead, R. P. 976. Conjugated macrocycles. Part XXIV. A new type of cross-conjugated macrocycle, related to the azaporphins. *J. Chem. Soc.* **1952**, 5000-5007.

(29) Pawlowski, G.; Michael H. A convenient synthesis of octasubstituted phthalocyanines, Synthesis 1980, 287-289.

(30) Leznoff, C. C.; and Tse Wai Hall. The synthesis of a soluble, unsymmetrical phthalocyanine on a polymer support. *Tetr. Lett.* **1982**, *23*, 3023-3026.

(31) Wheeler, B. L.; Nagasubramanian, G.; Bard, A. J.; Schechtman, L. A.; Kenney, M. E. A silicon phthalocyanine and a silicon naphthalocyanine: synthesis, electrochemistry, and electrogenerated chemiluminescence. *J. Am. Chem. Soc.* **1984**, *106*(24), 7404-7410.

(32) Camenzind, M. J.; Craig L. H. Synthesis of 2, 3, 9, 10, 16, 17, 23, 24-octaethylphthalocyanine. *J. Heterocycl. Chem.* **1985**, *22*(2), 575-576.

(33) Leznoff, C. C.; Lam, H.; Marcuccio, S. M.; Nevin, W. A.; Janda, P.; Kobayashi, N.; Lever, A. B. P. A planar binuclear phthalocyanine and its dicobalt derivatives. *J. Chem. Soc.* **1987** (9), 699-701.

(34) Díaz-Moscoso, A.; Emond, E.; Hughes, D. L.; Tizzard, G. J.; Coles, S. J.; Cammidge, A. N. Synthesis of a class of core-modified aza-BODIPY derivatives. *J. Org. Chem*, **2014**, 79(18), 8932-8936.

(35) Tamaoki, T.; Nomoto, H.; Takahashi, I.; Kato, Y.; Morimoto, M.; Tomita, F. Staurosporine, a potent inhibitor of phospholipidCa^{++} dependent protein kinase. *Biochem. Biophys. Res. Commun.* **1986**, 135(2), 397-402.

(36) Oka, S.; Kodama, M.; Takeda, H.; Tomizuka, N.; Suzuki, H. Staurosporine, a potent platelet aggregation inhibitor from a Streptomyces species. *J. Agric. Food Chem.* **1986**, *50*(11), 2723-2727.

(37) Ferland, J. M.; Demerson, C. A.; Humber, L. G. (). Synthesis of derivatives of isoindole and of pyrazino [2, 1-a] isoindole. *Can. J. Chem.* **1985**, *63*(2), 361-365.

(38) Linden, M.; Hadler, D.; Hofmann, S. Randomized, double-blind, placebo-controlled trial of the efficacy and tolerability of a new isoindoline derivative (DN-2327) in generalized anxiety. *Hum Psychopharm Clin*. **1997**, *12*(5), 445-452.

(39) Zhuang, Z. P.; Kung, M. P.; Mu, M.; Kung, H. F. Isoindol-1-one Analogues of 4-(2-methoxyphenyl)-1-[2-[N-(2-pyridyl)-p-iodobenzamido] ethyl] piperazine (p-MPPI) as 5-HT1A Receptor Ligands. *J. Med. Chem.* **1998**, *41*(2), 157-166.

(40) Zhu, X.; Greig, N. H.; Sheng Yu, Q.; Utsuki, T.; Holloway, H. W.; Lahiri, D.; Brossi, A. Synthesis of 3-alkylidene-isoindolinones via sulphide contraction. *Heterocycles*, **2004**, *64*, 93-99.

(41) Kundu, N. G.; Khan, M. W. Palladium-Catalysed Heteroannulation with Terminal Alkynes: a Highly Regio-and Stereoselective Synthesis of (*Z*)-3-Aryl (alkyl)idene Isoindolin-1-ones. *Tetrahedron*, **2000**, *56*(27), 4777-4792.

(42) Hendi, M. S.; Natalie Jr, K. J.; Hendi, S. B.; Campbell, J. A.; Greenwood, T. D.; Wolfe, J. F. Aromatic heteroannulation via ortho lithiation-cyclization of N-acyl-2-bromobenzamides. *Tetrahedron Lett.* **1989**, *30*(3), 275-278.

(43) Chen, X.; Ge, F. F.; Lu, T.; Zhou, Q. F. Stereoselective synthesis of 3-methyleneisoindolin-1-ones via base-catalyzed intermolecular reactions of electron-deficient alkynes with N-hydroxyphthalimides. *J. Org. Chem*. **2015**, *80*(6), 3295-3301.

(44) Shen, S.; Xu, X.; Lei, M.; Hu, L. Novel one-pot synthesis of 2-substituted 3-alkoxyisoindolin-1-imine derivatives from 2-cyanobenzaldehyde, amine, and alcohol. *Synthesis*. **2012**, *44*(22), 3543-3549.

(45) Pham, K.; Zhang, Z.; Shen, S.; Ma, L.; Hu, L. A one-pot synthesis of isoindolin-1-imine derivatives. *Tetrahedron*. **2013**, *69*(51), 10933-10939.

(46) Hellal, M.; Cuny, G. D. (). Microwave assisted copper-free Sonogashira coupling/5-exo-dig cycloisomerization domino reaction: access to 3-(phenylmethylene) isoindolin-1-ones and related heterocycles. *Tetrahedron Lett.* **2011**, *52*(42), 5508-5511.

(47) Díaz-Moscoso, A.; Tizzard, G. J.; Coles, S. J.; Cammidge, A. N. Synthesis of *meso*-Substituted Tetrabenzotriazaporphyrins: Easy Access to Hybrid Macrocycles. *Angew. Chem. Int. Ed.* **2013**, *125*(41), 10984-10987.

(48) Remiro-Buenamañana, S.; Díaz-Moscoso, A.; Hughes, D. L.; Bochmann, M.; Tizzard, G. J.; Coles, S. J.; Cammidge, A. N. Synthesis of Meso-Substituted Subphthalocyanine-Subporphyrin Hybrids: Boron Subtribenzodiazaporphyrins. *Angew. Chem. Int. Ed.* **2015**, *54*(26), 7510-7514.

(49) Zheng, W.; Wang, B. B.; Li, C. H.; Zhang, J. X.; Wan, C. Z.; Huang, J. H.; You, X. Z. Asymmetric Donor-Acceptor-Type Benzo-Fused Aza-BODIPYs: Facile Synthesis and Colorimetric Properties. *Angew. Chem. Int. Ed.* **2015**, 127(31), 9198-9202.

(50) Bredereck, H.; Vollmann, H. W. Synthesen in der heterocyclischen Reihe, XV. Über 1-[3-Aryl-isoindolyl-(1)-imino]-3-aryl-1H-isoindole. *Ber. Dtsch. Chem. Ges.* **1972**, *105*(7), 2271-2283.

(51) Bandi, V.; Gobeze, H. B.; D'Souza, F. Ultrafast Photoinduced Electron Transfer and Charge Stabilization in Donor–Acceptor Dyads Capable of Harvesting Near-Infrared Light. *Chem.: Eur. J.* **2015**, *21*(32), 11483-11494.

(52) Lu, H.; Shimizu, S.; Mack, J.; Shen, Z.; Kobayashi, N. Synthesis and Spectroscopic Properties of Fused-Ring-Expanded Aza-Boradiazaindacenes. *Chem. Asian J.* **2011**, *6*(4), 1026-1037.

(53) Gresser, R.; Hummert, M.; Hartmann, H.; Leo, K.; Riede, M. Synthesis and characterization of near-infrared absorbing benzannulated aza-BODIPY dyes. *Chem.: Eur. J.* **2011**, *17*(10), 2939-2947.

(54) Zatsikha, Y. V.; Schrage, B. R.; Meyer, J.; Nemykin, V. N.; Ziegler, C. J. 1,3-Diylideneisoindolines: Synthesis, Structure, Redox, and Optical Properties. *J. Org. Chem*. **2019**, *84*, 6217-6222.

(55) Makarova, E. A.; Zatsikha, Y. V.; Newman, K. M. E.; Paidi, V. K.; Beletsky, V. A.; van Lierop, J.; Lukyanets, E. A.; Nemykin, V. N. Direct Synthesis of an Unprecedented Stable Radical of Nickel(II) 3,5-Bis(dimedonyl)azadiisoindomethene with Strong and Narrow Near-Infrared Absorption at λ∼1000 nm. *Inorg. Chem*. **2017**, *56*, 6052-6055.

(56) Macrae, C. F.; Bruno, I. J.; Chisholm, J. A.; Edgington, P. R.; McCabe, P.; Pidcock, E.; Rodriguez-Monge, L.; Taylor, R.; van de Streek, J.; Wood, P. A. Mercury CSD 2.0–new features for the visualization and investigation of crystal structures. *J. Appl. Cryst*. **2008**, *41*, 466-470.

(57) Groom, C. R.; Bruno, I. J.; Lightfoot, M. P.; Ward, S. C. The Cambridge Structural Database *Acta Cryst.* **2016**, *B72*, 171-179, DOI: 10.1107/S2052520616003954.

(58) Sun, Y.; Gai, L.; Wang, Y.; Qu, Z.; Lu, H. Dithienosilole extended BODIPYs: Synthesis and spectroscopic properties. *J. Porphyrins Phthalocyanines* **2019**, *23*, 664-670.

(59) El-Ali, H. A. A.; Jing, J.; Zhang, X. Solid-state emissive O-BODIPY dyes with bimodal emissions across red and near infrared region. *RSC Adv*. **2019**, *9*, 16246-16251.

(60) Wan, W.; Silva, M. S.; McMillen, C. D.; Creager, S. E.; Smith, R. C. Highly Luminescent Heavier Main Group Analogues of Boron-Dipyrromethene. *J. Am. Chem. Soc.* **2019**, *141*, 8703-8707.

(61) Cetindere, S.; Tumay, S. O.; Senocak, A.; Kilic, A.; Durmus, M.; Demirbas, E.; Yesilot, S. Novel pyrene-BODIPY dyes based on cyclotriphosphazene scaffolds: Synthesis, photophysical and spectroelectrochemical properties. *Inorg. Chim. Acta* **2019**, *494*, 132-140.

(62) Thakare, S.; Stachelek, P.; Mula, S.; More, A. B.; Chattopadhyay, S.; Ray, A. K.; Sekar, N.; Ziessel, R.; Harriman, A. Solvent-Driven Conformational Exchange for Amide-Linked Bichromophoric BODIPY Derivatives. *Chem. Eur. J.* **2016**, *22*, 14356-14366.

(63) Dick, J. E.; Poirel, A.; Ziessel, R.; Bard, A. J. Electrochemistry, Electrogenerated Chemiluminescence, and Electropolymerization of Oligothienyl-BODIPY Derivatives. *Electrochim. Acta* **2015**, *178*, 234-239.

(64) Tao, J.; Sun, D.; Sun, L.; Li, Z.; Fu, B.; Liu, J.; Zhang, L.; Wang, S.; Fang, Y.; Xu, H. Tuning the photo-physical properties of BODIPY dyes: Effects of 1, 3, 5, 7- substitution on their optical and electrochemical behaviours. *Dyes Pigm.* **2019**, *168*, 166-174.

(65) Huaulme, Q.; Fall, S.; Leveque, P.; Ulrich, G.; Leclerc, N. Pairing of α-Fused BODIPY: Towards Panchromatic n-Type Semiconducting Materials. *Chem. Eur. J.* **2019**, *25*, 6613-6620.

(66) Kawamata, Y.; Ito, S.; Furuya, M.; Takahashi, K.; Namai, K.; Hashimoto, S.; Roppongi, M.; Oba, T. Synthesis and properties of novel extended BODIPYs with rigid skeletons. *Tetr. Lett.* **2019**, *60*, 707-712.

(67) Gao, D.; Aly, S. M.; Karsenti, P.-L.; Brisard, G.; Harvey, P. D. Application of the boron center for the design of a covalently bonded closely spaced triad of porphyrin-fullerene mediated by dipyrromethane. *Dalton Trans.* **2017**, *46*, 6278-6290.

(68) Cantu, R.; Gobeze, H. B.; D'Souza, F. Synthesis and photochemical studies of a tris(4-iodophenoxy) subphthalocyaninato boron(III)-fulleropyrrolidine dyad. *J. Porphyrins Phthalocyanines* **2016**, *20*, 987-996.

(69) Bottari, G.; Trukhina, O.; Kahnt, A.; Frunzi, M.; Murata, Y.; Rodriguez-Fortea, A.; Poblet, J. M.; Guldi, D. M.; Torres, T. Regio-, Stereo-, and Atropselective Synthesis of C$_{60}$ Fullerene Bisadducts by Supramolecular-Directed Functionalization. *Angew. Chem., Int. Ed.* **2016**, *55*, 11020-11025.

(70) Agazzi, M. L.; Durantini, J. E.; Gsponer, N. S.; Durantini, A. M.; Bertolotti, S. G.; Durantini, E. N. Light-harvesting antenna and proton-activated photodynamic effect of a novel BODIPY-fullerene C$_{60}$ dyad as potential antimicrobial agent. *ChemPhysChem*. **2019**, *20*, 1110-1125.

(71) Yin, X.; Li, Y.; Zhu, Y.; Jing, X.; Li, Y.; Zhu, D. A highly sensitive viscosity probe based on ferrocene-BODIPY dyads. *Dalton Trans*. **2010**, *39* (41), 9929-9935.

(72) LaMaster, D. J.; Kaufman, N. E. M.; Bruner, A. S.; Vicente, M. G. H. Structure Based Modulation of Electron Dynamics in *meso*-(4-Pyridyl)-BODIPYs: A Computational and Synthetic Approach. *J. Phys. Chem. A.* **2018**, *122*, 6372-6380.

(73) Gouterman, M. Spectra of porphyrins. *J. Mol. Spectrosc*. **1961**, *6*, 138-163.

(74) Gouterman, M.; Wagnière, G. H.; Snyder, L. C. Spectra of porphyrins. II. Four-orbital model. *J. Mol. Spectrosc.* **1963**, *11*, 108-127.

(75) Bruker-AXS *APEX3 v2016.1-0*, Madison,Wisconsin, USA, **2016**.

(76) Sheldrick, G.M. A short history of *SHELX*. *Acta Cryst.* **2008**, *A64*, 112-122.

(77) Spek, A.L. Structure validation in chemical crystallography. *Acta Cryst.* **2009**, *D65*, 148-155.

(78) Bellizzi, M.; Foss, P. C. D.; Pelto, R.; Crundwell, G.; Brueckner, C.; Updegraff, J. B., III; Zeller, M.; Hunter, A. D. Crystal structure of 5,10,15,20-tetrakis(5'-methylthien-2'-yl)porphyrin, $C_{40}H_{30}N_4S_4$ *Z. Krist. – New Cryst. St.* **2004**, *219*, 129-131 DOI: 10.1524/ncrs.2004.219.2.129.

(79) Wagner, P.; Officer, D. L.; Kubicki, M. A flip-disorder in the structure of 3-[2-(anthracen-9-yl)ethenyl]thiophene *Acta Cryst.* **2006**, *E62*, o5745-o5747.

(80) Macrae, C. F.; Edgington, P. R.; McCabe, P.; Pidcock, E.; Shields, G. P.; Taylor, R.; Towler, M.; van de Streek, J., Mercury: visualization and analysis of crystal structures. *J. Appl. Cryst*. **2006**, *39*, 453-457.

SYNOPSIS TOC